Neuronal dystroglycan is necessary for formation and maintenance of functional CCK-positive basket terminals on pyramidal cells

Neuronal dystroglycan is necessary for formation and maintenance of functional CCK-positive basket terminals on pyramidal cells

Dystroglycan function at CCK-positive terminals

Simon Früh[1,5], Jennifer Romanos[1,5], Patrizia Panzanelli[2], Daniela Bürgisser[3], Shiva K. Tyagarajan[1,5], Kevin P. Campbell[4], Mirko Santello[1,5], Jean-Marc Fritschy[1,5]

[1]Institute of Pharmacology and Toxicology, University of Zurich, 8057 Zurich, Switzerland [2]Department of Neuroscience Rita Levi Montalcini, University of Turin, 10124 Turin, Italy [3]ETH Zurich, 8092 Zurich, Switzerland [4]Howard Hughes Medical Institute, Department of Molecular Physiology and Biophysics, Department of Neurology, The University of Iowa Roy J. and Lucille A. Carver College of Medicine, Iowa City, Iowa 52242, USA [5]Neuroscience Center Zurich, University of Zurich and ETH Zurich, 8057 Zurich, Switzerland

Corresponding author: Jean-Marc Fritschy, Institute of Pharmacology and Toxicology, Winterthurerstrasse 190, 8057 Zurich, Switzerland, fritschy@pharma.uzh.ch

Number of pages: 32

Number of figures: 11

Number of words, abstract: 240 introduction: 649 discussion: 1464

Conflict of interest: The authors declare no competing financial interests.

Acknowledgements: This work was supported by a University of Zurich Forschungskredit grant to SF, the Swiss National Science Foundation (grant 310030_146120 to JMF) and a Paul D. Wellstone Muscular Dystrophy Cooperative Research Center grant (1U54NS053672 to KPC). KPC is an investigator of the Howard Hughes Medical Institute. We thank Prof.

Peter Scheiffele and Prof. Stephan Neuhauss for scientific discussion and Dr. Tatjana Haenggi and Cornelia Schwerdel for genotyping.

Distinct types of GABAergic interneurons target different subcellular domains of pyramidal cells, thereby shaping pyramidal cell activity patterns. Whether the presynaptic heterogeneity of GABAergic innervation is mirrored by specific postsynaptic factors is largely unexplored. Here we show that dystroglycan, a protein responsible for the majority of congenital muscular dystrophies when dysfunctional, has a function at postsynaptic sites restricted to a subset of GABAergic interneurons. Conditional deletion of Dag1, encoding dystroglycan, in pyramidal cells caused loss of CCK-positive basket cell terminals in hippocampus and neocortex. PV-positive basket cell terminals were unaffected in mutant mice, demonstrating interneuron subtype-specific function of dystroglycan. Loss of dystroglycan in pyramidal cells had little influence on clustering of other GABAergic postsynaptic proteins and of glutamatergic synaptic proteins. CCK-positive terminals were not established at P21 in the absence of dystroglycan and were markedly reduced when dystroglycan was ablated in adult mice, suggesting a role for dystroglycan in both formation and maintenance of CCK-positive terminals. The necessity of neuronal dystroglycan for functional innervation by CCK-positive basket cell axon terminals was confirmed by reduced frequency of inhibitory events in pyramidal cells of dystroglycan-deficient mice and further corroborated by the inefficiency of carbachol to increase IPSC frequency in these cells. Finally, neurexin binding seems dispensable for dystroglycan function since knock-in mice expressing binding-deficient T190M dystroglycan displayed normal CCK-positive terminals. Taken together, we describe a novel function of dystroglycan in interneuron subtype-specific trans-synaptic signaling, revealing correlation of pre- and postsynaptic molecular diversity.

Significance statement

Dystroglycan, an extracellular and transmembrane protein of the dystrophin glycoprotein complex, is at the center of molecular studies of muscular dystrophies. Although its synaptic distribution in cortical brain regions is long established, function of dystroglycan in the synapse remained obscure. Using mice that selectively lack neuronal dystroglycan, we provide evidence that a subset of GABAergic interneurons requires dystroglycan for formation and maintenance of axonal terminals on pyramidal cells. As such, dystroglycan is the first postsynaptic GABAergic protein for which an interneuron terminal-specific function could be shown. Our findings also offer a new perspective on the mechanisms that lead to intellectual disability in muscular dystrophies without associated brain malformations.

Introduction

GABAergic interneurons, which provide the main source of inhibitory drive in the adult mammalian brain, form several distinct classes according to morphological, molecular and functional criteria (Fishell and Rudy, 2011). This specialization allows interneurons to adapt to different demands of postsynaptic targets and thereby control membrane excitability in a spatially and temporally precise manner (Klausberger and Somogyi, 2008). Most interneuron classes innervate only a specific subcellular domain of target cells, for example the axon initial segment, the cell soma or dendritic regions. Synaptic transmission from different interneuron subtypes has thus fundamentally different impact on the activity of postsynaptic cells. It might be advantageous to account for this diversity of GABAergic innervation with postsynaptic specializations matching the specific properties and plasticity mechanisms of synaptic terminals they are contacted from. Indeed, the GABAergic postsynaptic density (PSD) is characterized by a large molecular heterogeneity (Tyagarajan and Fritschy, 2014). However, little is known about such subtype-specific postsynaptic GABAergic adaptations.

Basket cells are GABAergic interneurons that specifically target the perisomatic region of principal neurons. In cerebral cortex and hippocampus, expression of parvalbumin (PV) or cholecystokinin (CCK) identifies basket cells as belonging to one of two non-overlapping groups (Freund and Katona, 2007). Although these two interneuron subtypes innervate the

same subcellular domain, they are distinguished by various traits (Bartos and Elgueta, 2012). Only CCK-positive basket cells express presynaptic cannabinoid receptors, enabling retrograde signaling of endocannabinoids to suppress GABA release. Different firing patterns, expression profiles and developmental origins further set the two subtypes apart. Therefore, it is conceivable that the two types of basket cells use different mechanisms for synapse formation and require a different set of postsynaptic proteins to exert their vastly different functions.

Dystroglycan (DG) is the central component of the dystrophin glycoprotein complex (DGC). The extracellular α-DG and transmembrane β-DG, generated by proteolytic cleavage of a single gene product, bind the large cytoplasmic protein dystrophin, which in turn can interact with actin filaments. α-DG, through its glycosyl side chains, can bind to extracellular matrix components. The crucial role of the DGC in muscle tissue was revealed by mutations affecting DGC components that lead to muscular dystrophies (McNally and Pytel, 2007). The DGC, albeit differing slightly in its molecular composition, is also expressed in the central nervous system by glial cells and neurons (Waite et al., 2012). Developmental brain malformations and intellectual disability, observed frequently in muscular dystrophies caused by DGC dysfunction, testify to the importance of this complex for brain function. The finding that the DGC is present in pyramidal cells as large, mostly perisomatic clusters postsynaptic to GABAergic terminals spurred interest in the synaptic function of the DGC (Lidov et al., 1990). Because reduced $GABA_AR$ immunoreactivity was found in a mouse model of Duchenne's muscular dystrophy (DMD), a function for the DGC in clustering of PSD components was posited (Knuesel et al., 1999; Vaillend et al., 2010). Despite the selective DGC subcellular distribution, biochemical interaction with presynaptic neurexins and the obligatory association of DG with GABAergic presynaptic terminals in neuronal cultures, the role of the DGC in trans-synaptic signaling was never systematically assessed (Sugita et al., 2001; Brunig et al., 2002).

We hypothesized that the diversity of GABAergic PSD composition is functionally related to the heterogeneity of GABAergic innervation. Due to its restricted distribution and known role

as a transmembrane complex, DG seemed ideally suited to address this issue. Ablation of DG specifically in pyramidal neurons allowed us to study the synaptic function of the DGC without confounding deficits in neuronal migration associated with loss of DG in other tissues. Using this approach, we demonstrate that the neuronal DGC plays an essential role in trans-synaptic signaling necessary for formation and maintenance of functional axon terminals from CCK-positive basket cells. Since the neuronal circuits depending on this signaling have been shown to be involved in major cognitive functions, our findings open new avenues in identifying the causes of intellectual disability in muscular dystrophies.

Materials and Methods

Animals. All mice were bred on C57BL/6 background at the Laboratory Animal Service Center (Schlieren, Zurich, Switzerland) and kept in standard housing with food and water provided *ad libitum*. Mice harboring loxP sites in exon 2 of *Dag1* were obtained from The Jackson Laboratory (Bar Harbor, ME). NEX-Cre transgenic mice were provided by Dr. Sandra Goebbels (Max-Planck-Institute of Experimental Medicine, Goettingen, Germany). *Dag1* T190M knock-in mice were provided by Dr. Kevin P. Campbell (Howard Hughes Medical Institute, Iowa City, IA). *Dag1* floxed mice were genotyped by PCR analysis using primers 5'-GGAGAGGATCAATCATGG-3' and 5'-CAACTGCTGCATCTCTAC-3'. Genotyping of NEX-Cre transgenic mice was performed as described (Goebbels et al., 2006). To obtain DG cKO and control mice, NEX-Cre$^{tg/+}$ / *Dag1*$^{loxP/+}$ mice were bred to NEX-Cre$^{+/+}$ / *Dag1*$^{loxP/loxP}$ mice. All experiments were approved by the veterinary office of the Canton of Zurich.

Western blotting. Adult DG cKO and control mice of both sexes were anaesthetized with pentobarbital (Nembutal; 50 mg/kg intraperitoneally) and sacrificed by decapitation. Cheek muscle was dissected on ice and transferred to lysis buffer (50 mM Tris (pH 7.6), 150 mM NaCl, 1% Triton X-100, Complete Mini Protease Inhibitor Cocktail [Roche, Rotkreuz, Switzerland]). Tissue was Dounce homogenized, sonicated and incubated on ice for 1h. Lysates were centrifuged at 50'000 RPM for 1h at 4 °C and supernatants were stored at -80 °C. For anti-α-DG blots, glycosylated proteins were enriched by incubating lysates with wheat

germ agglutinin (WGA) agarose beads (Vector Labs, Burlingame, CA) at 4 °C overnight (ON). Proteins were eluted with 300 mM N-Acetyl-glucosamine and stored at -20 °C. Laemmli buffer was added to WGA-enriched and non-enriched lysates (for loading control) and samples were run on 8% tris-glycine polyacrylamide gels. Proteins were transferred to polyvinylidene fluoride (PVDF) membranes. Mouse anti-α-DG (11H6C4; Millipore; 1:1000) and rabbit anti-actin (Sigma; 1:5000) antibodies were incubated in tris-buffered saline with 0.05% Tween 20 (TBST) including 5% Western Blocking Solution (Roche) ON at 4 °C. Membranes were washed 5 times in TBST. Horseradish peroxidase-coupled donkey secondary antibodies (1:20'000) were incubated for 1h at room temperature (RT) and membranes were washed again 5 times in TBST. SuperSignal West Pico Chemiluminescent Substrate (Thermo Fisher Scientific, Waltham, MA) was applied and membranes were developed on X-ray film (Fujifilm, Tokyo, Japan).

Tissue preparation for immunohistochemistry. DG cKO and control mice of both sexes at the age of 8 to 12 weeks were anaesthetized by intraperitoneal pentobarbital injection (Nembutal; 50 mg/kg) and perfused transcardially with ice-cold oxygenated artificial cerebrospinal fluid (ACSF; pH 7.4) for 2 min, as described (Notter et al., 2014). Brains were immediately dissected and fixed in 4% paraformaldehyde (PFA) for 100 min on ice. After rinsing in phosphate-buffered saline (PBS), brains were incubated in 30% sucrose (in PBS) at 4 °C ON. 50 µm thick coronal sections were cut from frozen blocks using a sliding microtome (HM400; Microm, Walldorf, Germany) and stored at -20 °C in antifreeze solution. Tissue preparation from P21 mice followed the same protocol with the following modifications: Mice were perfused with 4% PFA (after brief perfusion with PBS to rinse blood) and brains were post-fixed for 3h.

Immunohistochemistry. After rinsing once in PBS, sections were incubated in primary antibody solution (50 mM Tris, 150 mM NaCl, 0.2% Triton X-100, 2% normal goat serum (NGS), pH 7.4) with antibodies listed in Table 1. Primary antibodies were incubated at 4 °C ON, or for 3 days if DG or dystrophin was labelled. Sections were washed 3 times for 10 min in PBS and incubated in secondary antibody solution (50 mM Tris, 150 mM NaCl, 0.05%

Triton X-100, 2% NGS, pH 7.4) for 30 min at RT with secondary antibodies raised in goat. Antibodies conjugated to Alexa Fluor 488 and Alexa Fluor 647 (Invitrogen, La Jolla, CA) were diluted 1:1000 whereas antibodies conjugated to Cy3 (Jackson ImmunoResearch, West Grove, PA) were diluted 1:500. Sections were washed 3 times for 10 min in PBS and mounted on gelatin-coated slides using Fluorescence Mounting Medium (Dako, Carpinteria, CA).

Image analysis. Z-stack images (3 optical sections, 0.5 µm step size) were recorded of all specimens using confocal laser scanning microscopy (LSM 700, Carl Zeiss, Oberkochen, Germany). Images were taken using a 40x objective with a numerical aperture of 1.4 and had a pixel size of 112 x 112 nm^2. To reduce variability, 3-4 sections were imaged per mouse and cluster density values were averaged from these sections. All imaging parameters were kept constant between genotypes. For cluster analysis, maximum intensity projections were created from z-stacks and analyzed using ImageJ (NIH, Bethesda, MD). Representative example images were processed with Imaris (Bitplane, Belfast, UK).

Stereotactic injections. 8 to 10 weeks old mice transgenic for loxP in exon 2 of *Dag1* were anaesthetized with isoflurane (Attane; Piramal, Mumbai, India). After mice were head-fixed on a stereotactic frame (David Kopf Instruments, Tujunga, CA), a small longitudinal incision was made under continuous administration of isoflurane to reveal the skull. Bregma was identified and the skull was perforated unilaterally using a surgical drill at the following coordinates relative to Bregma: x = -1.9 mm, y = 1.6 mm. A glass pipette filled with virus solution was inserted into the brain to z = 1.5 mm. A total of 1 µL virus solution was injected using an automated injection pump in increments of 70 nL over 10 min. The pipette was removed and the incision sutured. Mice were injected intraperitoneally with 1 mg/kg buprenorphine (Temgesic; Essex Chemicals, Lucerne, Switzerland) and placed on a warm pad for recovery before returning to the home cage.

Virus. AAV8-CaMKIIa-mCherry-Cre (dot blot titer $4.7x10^{12}$ VG/mL) was purchased from the University of North Carolina Vector Core (Chapel Hill, NC).

Acute brain slice preparation. 5 to 6 weeks old DG cKO and control mice were briefly anaesthetized with isoflurane and decapitated. The brain was quickly removed and transferred to ice-cold solution containing 65 mM NaCl, 2.5 mM KCl, 1.25 mM NaH_2PO_4, 25 mM $NaHCO_3$, 7 mM $MgCl_2$, 0.5 mM $CaCl_2$, 25 mM glucose and 105 mM sucrose saturated with 95% O_2 and 5% CO_2. 350 µm-thick transverse slices containing the hippocampus were cut from the tissue block with a vibratome (Microm HM 650V, Thermo Scientific, Waltham, MA) and kept in oxygenated ACSF (315 mOsm) containing 125 mM NaCl, 2.5 mM KCl, 1.25 mM NaH_2PO_4, 25 mM $NaHCO_3$, 1 mM $MgCl_2$, 2 mM $CaCl_2$ and 25 mM glucose at 34 °C for 25 min and then at room temperature until use.

Electrophysiology and data analysis. For recording, individual slices were transferred to a recording chamber perfused with oxygenated ACSF solution (same as above) at a flow rate of 1 to 2 mL/min. Whole-cell recordings were made from hippocampal CA1 pyramidal neurons. Cells were first selected using oblique IR illumination with a BX51 microscope (40x water-immersion objective; Olympus, Tokyo, Japan). Subsequently, neurons were anatomically identified using a fluorescent dye (Alexa 488, 10 µM) included in the intracellular solution. The dye was excited with wLS broad-band LED illumination (488 nm) and images were acquired with Retiga R1 camera using Ocular software (Qimaging, Surrey, Canada). The cells were patched with borosilicate glass pipettes (2-5 MΩ) containing: 135 mM KCl, 10 mM HEPES, 10 mM sodium phosphocreatine, 4 mM Mg-ATP, 0.3 mM Na-GTP, pH 7.3 with KOH. Recordings were performed using Multiclamp 700B amplifier and data were acquired with a Digidata 1550A 16-bit board (all from Molecular Devices, Sunnyvale, CA). All experiments were performed at room temperature. Spontaneous inhibitory postsynaptic currents (sIPSC) were recorded from CA1 pyramidal cells clamped at a membrane voltage of -70 mV in the presence of 10 µM NBQX to block excitatory transmission. Recordings with unstable baseline or greater than -400 pA were rejected. Currents were filtered off-line using a Butterworth low-pass filter (2 kHz) and analyzed in 1 or 2 min bins using the Mini-Analysis Program 6.0.7 (Synaptosoft, Decatur, GA). For pharmacology, baseline was analyzed 2 minutes before the application of carbachol (CCh,

10 µM). To study the effect of CCh, 1-2 min bins were analyzed at least 8 minutes following the arrival of CCh into the bath. Recordings with leak increasing more than 100 pA and access resistance changing more than 30% between the beginning and the end of the recording were discarded. At least 100 events were analyzed for any condition in any experiment. Events were identified as sIPSC by setting the event detection threshold at least 2-fold the baseline noise level and by checking that events had (i) rise times faster than the decay time, (ii) rise times greater than 0.5 ms and (iii) decay times greater than 1.5 ms. Events not fitting the above parameters were rejected. Event amplitudes, inter-event intervals, rise and decay times were first averaged within each experiment and regrouped by condition. The frequencies were calculated from the inter-event intervals and the resulting means were averaged between experiments. Single cell properties (access resistance, membrane capacitance, etc.) were analyzed with Clampfit 10.5 (Axon instruments, Union City, CA). Graphs were done using Igor 6.37 software (Wavemetrics, Tigard, OR) and Illustrator 15.1.0 (Adobe, San José, CA).

Results

Use of NEX-Cre driver line for pyramidal cell-specific DG ablation

To study the role of neuronal DGC in the brain without gross morphological alterations, it is necessary to target DG in neurons but spare glial DG. For this reason, mice harboring loxP sites in *Dag1* were crossed to the NEX-Cre driver line, which exhibits an exclusively neuronal Cre recombinase expression pattern (Goebbels et al., 2006; Satz et al., 2010). In hippocampus and neocortex, NEX promoter-mediated Cre expression is restricted to pyramidal cells, the cell type displaying most prominent DG expression in the forebrain. DG conditional knockout mice (cKO; NEX-Cre$^{Tg/+}$, *Dag1*$^{loxP/loxP}$) showed reduced size compared to control mice (NEX-Cre$^{Tg/+}$, *Dag1*$^{loxP/+}$; Figure 1A). The smaller size was reflected in reduced body and brain weight (Figure 1B and C; 25.3 ± 1.0 g [mean ± SEM] versus 18.7 ± 1.0 g, t_{28}=4.670, p<0.001 and 473.1 ± 5.4 mg versus 436.4 ± 6.5 mg, t_{28}=4.381, p<0.001, unpaired t-tests). Although cKO mice were born in Mendelian proportions, in adulthood less than the expected 25% cKO were observed due to higher lethality of cKO mice (Figure 1D).

To exclude a contribution of muscular dystrophy to this phenotype because of Cre leakage in muscle cells, α-DG levels were examined by Western blotting of WGA-enriched muscle proteins. cKO mice showed similar levels of muscle α-DG as control mice (Figure 1E). As reported before, DG cKO mice retained proper lamination of hippocampus (Figure 1F) and neocortex (Figure 1G) according to NeuN and DAPI labeling (Satz et al., 2010). Cre expression was restricted to pyramidal cells in hippocampus and neocortex and was not detected in dentate gyrus granule cells of adult mice (Figure 1F and G) (Goebbels et al., 2006).

Efficiency and specificity of DG ablation was examined immunohistochemically in relevant brain regions. α-DG, β-DG and dystrophin can be detected immunohistochemically in large perisomatic clusters in CA1 pyramidal cells (Figure 2A) (Lidov et al., 1990; Knuesel et al., 1999). This characteristic immunolabeling was absent in DG cKO mice for DG and to the same extent for dystrophin, showing that dystrophin needs DG for synaptic clustering *in vivo*. In neocortex, perisomatic distribution of α-DG, β-DG and dystrophin was replaced by diffuse unspecific staining in neuropil in DG cKO mice (Figure 2B). Astrocyte endfeet are labeled prominently by antibodies to β-DG and dystrophin and this labeling was preserved in DG cKO mice, as expected from neuron-specific Cre expression (asterisks in Figure 2A and B). α-DG immunolabeling in dentate gyrus granule cells showed the same clustered distribution in both genotypes (Figure 2C). The transient NEX promoter activity in these cells during early postnatal development might not be sufficient to achieve recombination (Goebbels et al., 2006). Alternatively, loss of DG during early development might be of little consequence in adulthood because of DG expression by granule cells that were born later. To further demonstrate specificity of NEX-induced DG ablation, striatum was selected as a control region. As expected, the characteristic sparse α-DG labeling persisted in striatum of DG cKO mice (Figure 2D).

Loss of neuronal DG results in minor alterations in GABAergic PSD protein clustering

Dependence of GABAergic postsynaptic density (PSD) proteins on the DGC for synaptic clustering was suggested because of the subcellular localization of the DGC, its molecular

interactions and because a reduction in $GABA_AR$ clustering was observed in mice lacking full-length dystrophin (Knuesel et al., 1999; Sumita et al., 2007; Waite et al., 2012). However, requirement of DG for clustering of GABAergic postsynaptic proteins was never systematically tested *in vivo*. We hypothesized that loss of neuronal DG affects neuroligin 2 (NL2) clustering, which might be important for clustering of $GABA_ARs$ at perisomatic synapses through its interaction with gephyrin (Poulopoulos et al., 2009; Panzanelli et al., 2011). DG cKO and control mice were analyzed for changes in clustering of these markers in CA1 pyramidal layer. As previously reported (Knuesel et al., 1999; Brunig et al., 2002; Levi et al., 2002), extensive colocalization of α-DG and dystrophin was observed with GABAergic markers, with a minority of DGC clusters showing no colocalization (Figure 3A and B; arrowheads and arrows, respectively). Visual examination of GABAergic markers revealed no obvious differences between genotypes (Figure 3A-C). However, quantification of cluster density and size showed a significant decrease of $GABA_AR$ α1 subunit size in cKO accompanied by an increase of $GABA_AR$ α2 subunit density (Figure 3D and F). No changes were observed in $GABA_AR$ γ2 subunit and gephyrin clustering (Figure 3E and H), indicating that total synaptic $GABA_AR$ content might be unchanged whereas α subunit composition is altered by loss of DG. Surprisingly, NL2 clustering was barely affected in cKO mice, showing no difference in density and only a slight but significant reduction in cluster size (Figure 3G). Neuronal DGC is also dispensable for normal colocalization of $GABA_AR$ γ2 subunit with gephyrin and of α1 subunit with NL2 (Figure 3I). Furthermore, dystrophin was suggested to be important for anchoring synArfGEF at GABAergic PSDs (Fukaya et al., 2011). Although dystrophin clustering is lost in DG cKO mice, synArfGEF distribution remained almost unchanged in CA1 pyramidal layer of cKO mice (Figure 3J).

Neuronal DG ablation leads to selective loss of markers of CCK-positive basket cell terminals

Many binding partners of α-DG have been identified, among them the presynaptic neurexins (Sugita et al., 2001). Taken together with the observation that DG is always apposed to GABAergic presynaptic terminals in primary neuronal culture, a trans-synaptic function for

DG seemed probable (Brunig et al., 2002). We therefore probed DG cKO and control brains tissue with antibodies to presynaptic GABAergic markers. Perisomatic GABAergic terminals can be attributed to parvalbumin (PV)- or cholecystokinin (CCK)-positive interneurons, which are labeled by PV / synaptotagmin 2 (Syt2) and CCK8 / VGluT3 / cannabinoid receptor 1 (CB1), respectively. We found that markers for presynaptic terminals from CCK-positive interneurons were virtually absent in CA1 pyramidal layer of DG cKO mice (Figure 4A-D, G, I and K). Still, like in control mice, CCK-positive cell somata were occasionally observed in cKO CA1 pyramidal layer, and these were often covered with VGluT3-positive boutons (arrowheads in Figure 4A). Syt2 and PV immunolabeling were still present in typical punctate distribution in the pyramidal layer of cKO mice (Figure 4A-D, H and J), demonstrating specific requirement of DG for formation of presynaptic terminals from CCK-positive interneurons. Preferential apposition of DG to CCK-positive interneuron terminals might be expected from this finding. However, apposition of DG to VGluT3 as well as to PV suggests no such distinction, at least at the resolution of conventional confocal laser scanning microscopy (arrowheads in C). Still, as percentage of presynaptic immunofluorescence apposed to DG, VGluT3 showed more complete overlap with DG, indicating PV apposition to DG might be caused by mere abundance of PV immunofluorescence in the pyramidal layer (data not shown). Loss of CCK-positive interneuron terminals extended from CA3 to CA1 (Figure 4E). Surprisingly, no corresponding reduction in VGAT puncta was observed (Figure 4F).

Because the DGC is prominently expressed by pyramidal cells in the neocortex, it seemed likely that CCK-positive interneuron terminals in neocortex are also compromised by loss of neuronal DG. Indeed, CCK8 and CB1 immunolabeling was strongly reduced in primary somatosensory cortex (S1) of DG cKO mice whereas PV staining was unchanged (apart from a minute difference in size; Figure 5). VGluT3 puncta density was not decreased in neocortex of DG cKO mice, in agreement with histological studies showing VGluT3 is present mostly in serotonergic fibers in this brain area (Figure 5B and G)(Schafer et al., 2002). As in hippocampus, reduction of CCK-positive terminals was not paralleled by a decrease of VGAT puncta (Figure 5A and E). Markers for CCK-positive terminals were

reduced uniformly across all cortical layers and in all regions of the neocortex which were examined (Figure 5D).

Satz et al. (2010) have reported blunted long-term potentiation in CA1 pyramidal cells of mice with NEX-Cre-mediated DG ablation. To exclude that loss of CCK-positive interneuron terminals represents compensatory changes to large glutamatergic alterations, glutamatergic markers were examined as a proxy for integrity of glutamatergic synapses (Figure 6). Clustering of the postsynaptic glutamatergic markers PSD-95 and bassoon did not differ significantly between genotypes (Figure 6A and B) and neither did VGluT1 immunolabeling (Figure 6C). Furthermore, the portion of PSD-95 clusters apposed to VGluT1 was similar in both genotypes (Figure 6D).

Formation and maintenance of CCK-positive basket cell terminals require neuronal DG

DG expressed by pyramidal cells might have a function in synapse formation or in guidance of a subset of axons, similar to its role in the spinal cord (Wright et al., 2012). Alternatively, a function in maintenance of synapses through continuous trans-synaptic signaling is conceivable. If neuronal DG is crucial for synapse formation of CCK-positive terminals, these boutons should be reduced to the same degree as in adults at a time point right after initial synaptogenesis. Following this reasoning, we examined CCK-positive terminals of 21-day-old DG cKO and control mice in CA1 pyramidal layer. Indeed, VGluT3 puncta were largely missing also at this stage of development whereas immunostaining of PV-positive terminals was not significantly different between genotypes (Figure 7).

Although this finding indicates that synapse formation of functional CCK-positive terminals depends on DG, it does not rule out a role for DG in maintaining already formed connections. In order to assess this putative function of DG in synapse maintenance, we ablated DG long after developmental synapse formation, by viral delivery of Cre to adult mice carrying one or both floxed *Dag1* alleles. AAV8-CaMKII-mCherry-Cre was stereotactically injected unilaterally into the CA1 region and mice sacrificed at 14, 28, 42 or 84 days post injection (dpi; Figure 8A and C). At 14 dpi, Cre as well as mCherry fluorescence were clearly visible (Figure 8B). Loss of β-DG staining at 28 dpi in homozygously floxed mice indicated efficient

recombination of loxP sites (Figure 8D). In heterozygously floxed mice only a moderate reduction of β-DG labeling was observed, suggesting one wildtype allele is sufficient to sustain the bulk of DG expression. Because dystrophin immunostaining revealed a reduction that mirrored β-DG, and in addition showed lower background, dystrophin was used to assess DGC loss at subsequent time points (Figure 8E-G). Examination of VGluT3-positive terminals at 28 dpi in Cre-expressing regions of CA1 pyramidal layer revealed a moderate but significant reduction of VGluT3 puncta density and size in homozygously floxed mice compared to contralateral side as well as compared to the ipsilateral side of heterozygously floxed mice (Figure 8H). VGluT3-positive terminals in heterozygous mice were not affected. Compromised VGluT3 immunolabeling was also found at later time points in homozygous mice, and the effect became more prominent with increased time after injection (Figure 8I and J). Together, these results provide strong evidence for a role of DG both in synapse formation and in retrograde trans-synaptic signaling for maintenance of CCK-positive terminals.

Absence of CCK-positive basket cell terminals due to DG ablation impacts pyramidal cell inhibitory input and response to cholinergic activation

If axon terminals from CCK-positive basket cells are indeed lost in DG ablated mice, this should be reflected by functional changes of pyramidal cell inhibitory input. To test this hypothesis, acute slices were prepared from adult DG cKO and control brains and used for patch-clamp electrophysiological recordings from morphologically identified CA1 pyramidal cells (Figure 9). With inhibitors of glutamatergic transmission present in the bath, occurrence of spontaneous inhibitory postsynaptic currents (sIPSCs) was probed in both genotypes. As anticipated from immunohistological changes, sIPSC frequency in DG cKO was reduced to about half of that in control slices (Figure 9; 8.71 ± 1.52 Hz versus 4.46 ± 0.90 Hz, t_{26}=2.214, p=0.036, unpaired t-test). Furthermore, DG cKO pyramidal cells were marked by a significantly smaller sIPSC amplitude than that of control cells (61.49 ± 7.90 pA versus 39.18 ± 2.39 pA, t_{26}=2.374, p=0.025, unpaired t-test). No significant differences were found between genotypes in sIPSC rise and decay times (rise time 1.73 ± 0.09 ms versus 1.63 ±

388 0.12 ms, t_{26}=0.664, p=0.512, unpaired t-test; decay time 14.84 ± 0.64 ms versus 14.21 ± 0.53
389 ms, t_{26}=0.717, p=0.480, unpaired t-test).
390 The differences observed in baseline sIPSCs could be due to a general reduction of
391 inhibitory transmission instead of interneuron subtype-specific loss of terminals. In order to
392 gain insight into the origin of reduced inhibitory transmission in DG cKO pyramidal cells, we
393 examined the effect of the acetylcholine receptor agonist carbachol on inhibitory currents. In
394 slices, carbachol exposure leads to an increase of perisomatic inhibitory transmission in
395 pyramidal cells, which is mediated by direct excitation of CCK-positive interneurons (Nagode
396 et al., 2014). Given that CB1 receptor-containing terminals are required for increased
397 inhibitory transmission after application of carbachol, this effect should be absent in DG cKO
398 mice, if CCK-positive basket terminals are indeed non-functional in these mice. Carbachol
399 was bath-applied to DG cKO and control acute slices from which sIPSCs were recorded in
400 CA1 pyramidal cells. In control slices, carbachol led to a robust increase in sIPSC frequency
401 within minutes after application (Figure 10A-C; frequency: 6.15 ± 1.45 Hz versus 10.53 ±
402 2.47 Hz, t_7=3.522, p=0.010; amplitude: 63.36 ± 8.84 pA versus 70.35 ± 12.59 pA, t_7=0.943,
403 p=0.377; paired t-tests). However, no statistically significant effect of carbachol was observed
404 in DG cKO pyramidal cells (Figure 10D-F; frequency: 3.45 ± 0.75 Hz versus 4.47 ± 1.56 Hz,
405 t_6=0.797, p=0.456; amplitude: 45.70 ± 4.17 pA versus 53.03 ± 5.00 pA, t_6=1.239, p=0.262;
406 paired t-tests). Together with the results from baseline recordings and immunohistochemical
407 analysis, these findings strongly argue that functional connectivity between CCK-containing
408 basket cells and pyramidal cells is lost in DG-ablated mice.
409 **Persistence of CCK-positive terminals in DG T190M knock-in mice suggests trans-**
410 **synaptic DG function is independent of neurexin binding**
411 The intriguing finding that DG is required for formation and maintenance of CCK-positive
412 terminals calls for an assessment of the clinical significance of this observation. In a
413 subgroup of dystroglycanopathies, intellectual disability, although severe, is not accompanied
414 by neuronal migration deficits (Godfrey et al., 2007). *Dag1* T190M knock-in mice are a model
415 of one such form of dystroglycanopathy and resemble the symptoms found in patients with

the corresponding mutation (Dincer et al., 2003; Hara et al., 2011). Interestingly, this mutation abolishes binding of DG to neurexin, a putative presynaptic DG binding partner. We compared markers of CCK-positive terminals in CA1 pyramidal layer of homozygous *Dag1* T190M mice to wildtype mice (Figure 11). Surprisingly, both VGluT3 and CB1 puncta were indistinguishable between *Dag1* T190M and wildtype mice. Weaker and more diffuse labeling in *Dag1* T190M mice using the α-DG glycosylation-specific antibody 11H6 confirmed that this mutation affects glycosylation of neuronal DG (Figure 11B). Apposition of β-DG to PV or VGluT3-positive terminals was not changed by T190M mutation (Figure 11E). Therefore, DG function for CCK-positive terminals is likely neurexin-independent, which suggests a novel presynaptic receptor might be involved in this trans-synaptic connection.

Discussion

Our experiments have yielded five main findings about the synaptic function of DG. Ablation of neuronal DG, which also hindered synaptic clustering of dystrophin, led only to minor changes in clustering of GABAergic PSD proteins. These alterations might reflect compensatory changes to the massive presynaptic defects found in DG-deficient mice. Importantly, DG synaptic function is interneuron subtype-specific since loss of synaptic markers was restricted to CCK-expressing basket cell terminals. Formation and maintenance of these synapses required neuronal DG, indicating that trans-synaptic signaling is important both at the time of developmental synaptogenesis and continuously during adulthood. Function of CCK-positive basket cell terminals was likely compromised along with specific marker expression, since loss of DG resulted in a reduced baseline spontaneous inhibitory activity in pyramidal cells that could not be increased by carbachol. Finally, post-phosphorylation glycosylation of DG is not necessary for CCK-positive synapse formation because *Dag1* T190M knock-in mice showed normal CCK-positive terminals, suggesting that presynaptic receptors other than neurexins might be involved in DG trans-synaptic function.

Postsynaptic GABAergic alterations ascribed to DGC deficits may be secondary to innervation defects

Ablation of DG in primary hippocampal culture has revealed that DG is not necessary for GABAergic synapse formation and for clustering of main GABAergic PSD proteins, including $GABA_A$Rs (Levi et al., 2002). Yet, involvement of the DGC in clustering of GABAergic postsynaptic proteins was supported by several lines of evidence. Mdx mice, used as a DMD model because of their lack of full-length dystrophin, were shown to have reduced $GABA_A$R (but not gephyrin) clustering in the hippocampus CA1 region (Knuesel et al., 1999). Overexpression of a shorter dystrophin construct *in vivo* rescued the decrease of $GABA_A$R cluster density and size, adding to the notion that dystrophin loss directly caused $GABA_A$R clustering defects (Vaillend et al., 2010). Neuroligin 2 (NL2) was shown to biochemically interact with dystrophin over the intracellular synaptic scaffolding molecule S-SCAM (Sumita et al., 2007). Furthermore, a functional connection between the DGC and NL2 is suggested by the observation that in $GABA_A$R α2 subunit KO mice NL2 clustering is only compromised in dendritic but not in perisomatic areas (Panzanelli et al., 2011). The modest increase in $GABA_A$R α2 subunit density and decrease in $GABA_A$R α1 subunit size found in the present study does not correspond to the findings in mdx mice, in which both subunits cluster less efficiently than in wildtype mice (Knuesel et al., 1999; Vaillend et al., 2010). Rather, these alterations might reflect a subunit composition change because $GABA_A$R γ2 subunit clusters were not affected by ablation of DG (except for a minute reduction in cluster size, which might be a reflection of reduced $GABA_A$R α1 subunit cluster size). The finding that gephyrin clustering was unchanged in DG cKO mice further supports the conclusion that overall clustering of synaptic $GABA_A$R subunits was not influenced by neuronal DG loss. The discrepancy between our results and published data from mdx mice might be explained by different roles of dystrophin isoforms at the GABAergic PSD. Short dystrophin isoforms still present in the mdx model might, by binding to DG, cause the reduction in synaptic $GABA_A$R clustering. It is worth noting that the α2 subunit of $GABA_A$Rs, which is localized preferentially at CCK-positive synapses (Nyiri et al., 2001), does not require the DGC or CCK-positive

terminals for clustering. The DGC is thus likely involved in targeting the α2 subunit to synapses apposed to CCK-positive terminals but clustering mechanisms seem to be DGC-independent. NL2 clustering was intact in DG cKO mice, apart from a slight decrease in cluster size. Therefore, the notion of the DGC as an obligatory stabilizer of postsynaptic NL2 clustering by mutual interaction with S-SCAM does not hold. Similarly, a role for the DGC in clustering the dystrophin-interacting protein synArfGEF at GABAergic synapses was suggested (Fukaya et al., 2011). Not excluding a contribution of the DGC to synArfGEF function by clustering additional signaling proteins, synArfGEF does not rely on the DGC to form clustered, presumably synaptic structures.

In the light of the dramatic changes in GABAergic innervation due to DG loss, an indirect presynaptic contribution to reduced postsynaptic clustering in dystrophin-deficient models should be considered. This hypothesis is supported also by the finding of reduced CCK-positive basket cell markers in mdx mice, suggesting that dystrophin plays part in trans-synaptic signaling (Krasowska et al., 2014). The role of dystrophin in clustering signaling proteins at CCK-positive terminals is still unexplored, but might include retrograde signaling by nitric oxide synthase. Resolution of conventional confocal laser scanning microscopy is not sufficient to conclusively answer whether the DGC is restricted to synapses from CCK-positive basket cells. Although apposition of DG to PV- and CCK-positive terminals was found with approximately equal frequency (Figure 11E), the percentage of CCK-positive terminals apposed to DG was higher than that of PV-positive terminals (data not shown; Figure 4C and 7A). Therefore, it seems likely that the DGC localizes preferentially postsynaptic to CCK-positive terminals to regulate synapse formation and function.

Basket cell type specificity of DG function implies specificity of trans-synaptic interaction with presynaptic binding partner

The selective dependence of the CCK-containing subtype of basket cells on neuronal DG for innervating target cells is a major finding of our study and has far-reaching implications. The DGC indeed acts as a trans-synaptic complex in central synapses, suggesting that presynaptic, rather than extracellular binding partners, enable DGC function in this context.

Any such presynaptic adhesion molecule would have to be specifically localized at CCK-positive terminals. Interestingly, differential splicing of neurexins in PV- and CCK-expressing basket cells was recently reported (Fuccillo et al., 2015). Transcripts lacking neurexin1α alternative splice inserts 2 and 4, which prevent α-DG binding to LSM domains 2 and 6, respectively, were only found in CCK-positive basket cells (Sugita et al., 2001; Reissner et al., 2014; Fuccillo et al., 2015). This neurexin isoform-specificity of basket cell subtypes would provide a mechanism for selective dependence of CCK-positive basket terminals on DG. However, we found terminals from CCK-positive basket cells to be intact in *Dag1* T190M knock-in mice. DG containing the T190M mutation was found to lose neurexin binding capacity (Hara et al., 2011). This finding thus suggests that a novel presynaptic DG binding partner might be specifically localized at CCK-positive terminals. But because the diversity of neurexin isoforms was not considered in DG T190M binding assays, the possibility of a specific neurexin-DG trans-synaptic complex at CCK-positive terminals remains.

Continuous trans-synaptic signaling required for maintenance of CCK-positive terminals might reflect novel plasticity mechanism

Stopping trans-synaptic signaling mediated by the DGC by ablating DG in adulthood led to a decrease of CCK-positive terminals within weeks. This unexpected result implies that DG function goes beyond a potential role in validating newly formed synapses from CCK-positive basket cells. In addition to clustering signaling molecules at these synapses, our findings open the possibility that the DGC, by forming a trans-synaptic complex, is a direct target to regulate abundance of CCK-positive terminals. β-DG is a substrate of MMP-9 in a neuronal activity-dependent manner (Yamada et al., 2001; Kaczmarek et al., 2002; Michaluk et al., 2007). Cleavage of DG might therefore represent a physiological interneuron subtype-specific plasticity mechanism. In striking agreement with this hypothesis, CCK-positive terminals are selectively lost in a model of temporal lobe epilepsy (Wyeth et al., 2010).

Decreased inhibitory input to pyramidal cells in DG-ablated cells confirms functional significance of DG signaling for CCK-positive terminals

The possibility that loss of CCK-specific markers in DG cKO mice is only due to inability of terminals to differentiate was ruled out by the finding that DG-ablated pyramidal cells receive reduced inhibitory drive. Along with sIPSC frequency, amplitude was markedly reduced, possibly reflecting mistargeting of $GABA_A$Rs in the absence of the DGC. Genesis of carbachol-induced increase of inhibitory currents is not fully understood but involves Gad2-positive rather than PV-positive interneurons in the CA1 region (Nagode et al., 2014). Since the group of Gad2-expressing interneurons includes CCK-positive basket cells and carbachol-induced currents are sensitive to depolarization-induced suppression of inhibition, our results add to the notion that CCK-positive basket cells play a crucial role in carbachol-induced activity. Activity patterns elicited by carbachol correlate with behaviorally relevant theta oscillations. Mechanisms of theta oscillation generation should thus be considered in future investigations of the etiology of intellectual disability associated with muscular dystrophies.

Conclusions

Our investigation of the role of neuronal DG in GABAergic synapses has revealed a surprising interneuron type-specific function of DG in trans-synaptic signaling. It has shown that GABAergic postsynaptic diversity is functionally related to interneuron subtype heterogeneity and supports the emerging notion of a cell type-specific molecular code of synapse formation. Future studies will have to further characterize signaling and plasticity enabled by the DGC and delineate its behavioral consequences. Taking the interneuron-specific role of DG into consideration will help elucidate the mechanisms underlying intellectual disability observed in muscular dystrophies without developmental brain malformations.

References

Bartos M, Elgueta C (2012) Functional characteristics of parvalbumin- and cholecystokinin-expressing basket cells. J Physiol 590:669-681.

Brunig I, Suter A, Knuesel I, Luscher B, Fritschy JM (2002) GABAergic terminals are required for postsynaptic clustering of dystrophin but not of GABA(A) receptors and gephyrin. J Neurosci 22:4805-4813.

Dincer P, Balci B, Yuva Y, Talim B, Brockington M, Dincel D, Torelli S, Brown S, Kale G, Haliloglu G, Gerceker FO, Atalay RC, Yakicier C, Longman C, Muntoni F, Topaloglu H (2003) A novel form of recessive limb girdle muscular dystrophy with mental retardation and abnormal expression of alpha-dystroglycan. Neuromuscul Disord 13:771-778.

Fishell G, Rudy B (2011) Mechanisms of inhibition within the telencephalon: "where the wild things are". Annu Rev Neurosci 34:535-567.

Freund TF, Katona I (2007) Perisomatic inhibition. Neuron 56:33-42.

Fritschy JM, Mohler H (1995) GABAA-receptor heterogeneity in the adult rat brain: differential regional and cellular distribution of seven major subunits. J Comp Neurol 359:154-194.

Fuccillo MV, Foldy C, Gokce O, Rothwell PE, Sun GL, Malenka RC, Sudhof TC (2015) Single-Cell mRNA Profiling Reveals Cell-Type-Specific Expression of Neurexin Isoforms. Neuron 87:326-340.

Fukaya M, Kamata A, Hara Y, Tamaki H, Katsumata O, Ito N, Takeda S, Hata Y, Suzuki T, Watanabe M, Harvey RJ, Sakagami H (2011) SynArfGEF is a guanine nucleotide exchange factor for Arf6 and localizes preferentially at post-synaptic specializations of inhibitory synapses. J Neurochem 116:1122-1137.

Godfrey C et al. (2007) Refining genotype phenotype correlations in muscular dystrophies with defective glycosylation of dystroglycan. Brain 130:2725-2735.

Goebbels S, Bormuth I, Bode U, Hermanson O, Schwab MH, Nave KA (2006) Genetic targeting of principal neurons in neocortex and hippocampus of NEX-Cre mice. Genesis 44:611-621.

Hara Y, Balci-Hayta B, Yoshida-Moriguchi T, Kanagawa M, Beltran-Valero de Bernabe D, Gundesli H, Willer T, Satz JS, Crawford RW, Burden SJ, Kunz S, Oldstone MB, Accardi A,

577 Talim B, Muntoni F, Topaloglu H, Dincer P, Campbell KP (2011) A dystroglycan mutation
578 associated with limb-girdle muscular dystrophy. N Engl J Med 364:939-946.
579 Kaczmarek L, Lapinska-Dzwonek J, Szymczak S (2002) Matrix metalloproteinases in the
580 adult brain physiology: a link between c-Fos, AP-1 and remodeling of neuronal connections?
581 Embo J 21:6643-6648.
582 Klausberger T, Somogyi P (2008) Neuronal diversity and temporal dynamics: the unity of
583 hippocampal circuit operations. Science 321:53-57.
584 Knuesel I, Mastrocola M, Zuellig RA, Bornhauser B, Schaub MC, Fritschy JM (1999) Short
585 communication: altered synaptic clustering of GABAA receptors in mice lacking dystrophin
586 (mdx mice). Eur J Neurosci 11:4457-4462.
587 Krasowska E, Zablocki K, Gorecki DC, Swinny JD (2014) Aberrant location of inhibitory
588 synaptic marker proteins in the hippocampus of dystrophin-deficient mice: implications for
589 cognitive impairment in duchenne muscular dystrophy. PLoS One 9:e108364.
590 Levi S, Grady RM, Henry MD, Campbell KP, Sanes JR, Craig AM (2002) Dystroglycan is
591 selectively associated with inhibitory GABAergic synapses but is dispensable for their
592 differentiation. J Neurosci 22:4274-4285.
593 Lidov HG, Byers TJ, Watkins SC, Kunkel LM (1990) Localization of dystrophin to
594 postsynaptic regions of central nervous system cortical neurons. Nature 348:725-728.
595 McNally EM, Pytel P (2007) Muscle diseases: the muscular dystrophies. Annu Rev Pathol
596 2:87-109.
597 Michaluk P, Kolodziej L, Mioduszewska B, Wilczynski GM, Dzwonek J, Jaworski J, Gorecki
598 DC, Ottersen OP, Kaczmarek L (2007) Beta-dystroglycan as a target for MMP-9, in response
599 to enhanced neuronal activity. J Biol Chem 282:16036-16041.
600 Nagode DA, Tang AH, Yang K, Alger BE (2014) Optogenetic identification of an intrinsic
601 cholinergically driven inhibitory oscillator sensitive to cannabinoids and opioids in
602 hippocampal CA1. J Physiol 592:103-123.

603 Notter T, Panzanelli P, Pfister S, Mircsof D, Fritschy JM (2014) A protocol for concurrent
604 high-quality immunohistochemical and biochemical analyses in adult mouse central nervous
605 system. Eur J Neurosci 39:165-175.
606 Nyiri G, Freund TF, Somogyi P (2001) Input-dependent synaptic targeting of alpha(2)-
607 subunit-containing GABA(A) receptors in synapses of hippocampal pyramidal cells of the rat.
608 Eur J Neurosci 13:428-442.
609 Panzanelli P, Gunn BG, Schlatter MC, Benke D, Tyagarajan SK, Scheiffele P, Belelli D,
610 Lambert JJ, Rudolph U, Fritschy JM (2011) Distinct mechanisms regulate GABAA receptor
611 and gephyrin clustering at perisomatic and axo-axonic synapses on CA1 pyramidal cells. J
612 Physiol 589:4959-4980.
613 Poulopoulos A, Aramuni G, Meyer G, Soykan T, Hoon M, Papadopoulos T, Zhang M,
614 Paarmann I, Fuchs C, Harvey K, Jedlicka P, Schwarzacher SW, Betz H, Harvey RJ, Brose N,
615 Zhang W, Varoqueaux F (2009) Neuroligin 2 drives postsynaptic assembly at perisomatic
616 inhibitory synapses through gephyrin and collybistin. Neuron 63:628-642.
617 Reissner C, Stahn J, Breuer D, Klose M, Pohlentz G, Mormann M, Missler M (2014)
618 Dystroglycan binding to alpha-neurexin competes with neurexophilin-1 and neuroligin in the
619 brain. J Biol Chem 289:27585-27603.
620 Satz JS, Ostendorf AP, Hou S, Turner A, Kusano H, Lee JC, Turk R, Nguyen H, Ross-Barta
621 SE, Westra S, Hoshi T, Moore SA, Campbell KP (2010) Distinct functions of glial and
622 neuronal dystroglycan in the developing and adult mouse brain. J Neurosci 30:14560-14572.
623 Schafer MK, Varoqui H, Defamie N, Weihe E, Erickson JD (2002) Molecular cloning and
624 functional identification of mouse vesicular glutamate transporter 3 and its expression in
625 subsets of novel excitatory neurons. J Biol Chem 277:50734-50748.
626 Sugita S, Saito F, Tang J, Satz J, Campbell K, Sudhof TC (2001) A stoichiometric complex of
627 neurexins and dystroglycan in brain. J Cell Biol 154:435-445.
628 Sumita K, Sato Y, Iida J, Kawata A, Hamano M, Hirabayashi S, Ohno K, Peles E, Hata Y
629 (2007) Synaptic scaffolding molecule (S-SCAM) membrane-associated guanylate kinase with

inverted organization (MAGI)-2 is associated with cell adhesion molecules at inhibitory synapses in rat hippocampal neurons. J Neurochem 100:154-166.

Tyagarajan SK, Fritschy JM (2014) Gephyrin: a master regulator of neuronal function? Nat Rev Neurosci 15:141-156.

Vaillend C, Perronnet C, Ros C, Gruszczynski C, Goyenvalle A, Laroche S, Danos O, Garcia L, Peltekian E (2010) Rescue of a dystrophin-like protein by exon skipping in vivo restores GABAA-receptor clustering in the hippocampus of the mdx mouse. Mol Ther 18:1683-1688.

Waite A, Brown SC, Blake DJ (2012) The dystrophin-glycoprotein complex in brain development and disease. Trends Neurosci 35:487-496.

Wright KM, Lyon KA, Leung H, Leahy DJ, Ma L, Ginty DD (2012) Dystroglycan organizes axon guidance cue localization and axonal pathfinding. Neuron 76:931-944.

Wyeth MS, Zhang N, Mody I, Houser CR (2010) Selective reduction of cholecystokinin-positive basket cell innervation in a model of temporal lobe epilepsy. J Neurosci 30:8993-9006.

Yamada H, Saito F, Fukuta-Ohi H, Zhong D, Hase A, Arai K, Okuyama A, Maekawa R, Shimizu T, Matsumura K (2001) Processing of beta-dystroglycan by matrix metalloproteinase disrupts the link between the extracellular matrix and cell membrane via the dystroglycan complex. Hum Mol Genet 10:1563-1569.

Legends

Figure 1. Characterization of NEX-Cre / *Dag1* conditional KO mice. A, Representative examples of NEX-Cre$^{Tg/+}$ / *Dag1*$^{loxP/+}$ (control) and NEX-Cre$^{Tg/+}$ / *Dag1*$^{loxP/loxP}$ (cKO) mice (4 months of age, siblings, both female). B, cKO mice exhibit reduced body weight compared to sibling control mice. C, Wet brain weight was lower in cKO mice than in controls. D, cKO mice exhibited a higher mortality rate than control mice, resulting in a frequency of cKO mice lower than the expected 25% at the age of 10 weeks. E, Similar levels of α-DG isolated from cheek muscle were found for cKO and control mice. F, Cre expression was restricted to pyramidal cells in the hippocampus of cKO and control mice. In adult mice, dentate gyrus

granule cells were not immunoreactive for Cre recombinase. NeuN and DAPI labeling show intact neuronal migration when NEX-Cre is used as driver line to ablate *Dag1*. G, In primary somatosensory cortex Cre expression was also restricted to pyramidal cells. No migratory deficits were found in the neocortex in cKO mice. ***p<0.001.

Figure 2. NEX-Cre-mediated ablation of dystroglycan leads to specific loss of dystrophin glycoprotein complex in pyramidal cells. A, Characteristic staining of α- and β-DG and dystrophin around CA1 pyramidal layer is lost in cKO mice. Labeling of β-DG and dystrophin in astrocyte end-feet is retained in cKO mice (asterisks). B, In primary somatosensory cortex layer 2/3, clustered labeling of DGC components around pyramidal cells is replaced by diffuse staining in the neuropil. Astrocyte end-feet labeling of β-DG and dystrophin is retained in cKO mice (asterisks). C, α-DG immunofluorescence in dentate gyrus is unaffected by NEX-Cre-mediated ablation of DG. D, α-DG expression in striatum is unaffected in cKO mice, confirming specificity of NEX-Cre expression to pyramidal cells. SR, stratum radiatum; SP, stratum pyramidale; ML, molecular layer; GCL, granule cell layer.

Figure 3. Loss of neuronal dystroglycan does not prohibit formation of GABAergic PSD but leads to minor changes in $GABA_AR$ subunit clustering. A-C, Triple immunofluorescence labeling of GABAergic postsynaptic markers in pyramidal layer of hippocampus CA1 area. The DGC is largely colocalized with α2 subunit and VGAT (A; arrowheads) but also with α1 subunit and NL2 (B; arrowheads). A minority of DGC clusters is not associated with GABAergic markers (A and B; arrows). D-H, Quantification of postsynaptic GABAergic markers in CA1 pyramidal cell layer. Cluster density and size are shown for $GABA_AR$ α1 (D), α2 (F) and γ2 (H) subunits and for gephyrin (E) and NL2 (G). A decrease of α1 subunit cluster size was accompanied by an increased α2 subunit cluster density. I, Colocalization of postsynaptic GABAergic markers was analyzed in cKO and control mice. Data represent the number of colocalized clusters as percentage of first mentioned marker. No significant differences in colocalization were found between genotypes. J, Clustering of synArfGEF was analyzed in CA1 pyramidal layer of DG cKO and control mice. Data points represent individual mice. **p<0.01, ***p<0.001 (see Table 2 for statistical tests).

Figure 4. Neuronal dystroglycan ablation leads to specific loss of terminals from CCK-positive basket cells on hippocampal pyramidal cells. A-D, Triple immunofluorescence labeling of presynaptic GABAergic markers in hippocampus CA1 area. A, In pyramidal layer, markers labeling CCK-positive basket cell terminals (CCK8, VGluT3) are missing around pyramidal cell bodies, but are still present on CCK-positive cell somata occasionally observed near the pyramidal layer (arrows). These VGluT3-positive boutons on CCK-positive somata were often immunopositive for synaptotagmin 2. In the pyramidal layer, immunostaining for synaptotagmin 2 remained in cKO mice. B1 and B2 show separated channels of insets in A. C, PV immunolabeling in CA1 pyramidal layer of DG cKO mice is indistinguishable from control. In CA1 pyramidal layer of control mice, the majority of α-DG clusters is either apposed to VGluT3 (arrow 1) or PV (arrow 2), but some clusters are not apposed to either marker (arrow 3). A minority of α-DG clusters showed apposition to both VGluT3 and PV (arrow 4). D, Along with CCK8 and VGluT3, CB1 staining is strongly reduced in CA1 pyramidal layer of DG cKO mice. E, Loss of CB1 immunofluorescence in DG cKO mice was observed from CA1 to CA3. F-K, Quantification of presynaptic GABAergic markers in CA1 pyramidal layer. No changes were found for VGAT (F) and PV-positive basket cell markers (H, J) between genotypes but cluster density and size of markers of CCK-positive basket cell terminals (G, I, K) were strongly reduced in DG cKO mice. Data points represent individual mice. ***$p<0.001$ (see Table 2 for statistical tests). SR, stratum radiatum; SP, stratum pyramidale.

Figure 5. Neuronal dystroglycan ablation leads to specific loss of terminals from CCK-positive basket cells on pyramidal cells in neocortex. A-C, Triple immunofluorescence labeling of GABAergic markers in layer 2/3 of primary somatosensory cortex (S1) of DG cKO and control mice. A, As in hippocampus, the majority of DG clusters is colocalized with pre- and postsynaptic GABAergic markers in neocortex. B, Neocortical PV and VGluT3 immunolabeling is not affected by loss of neuronal DG. C, CCK8 and CB1 immunofluorescence is strongly reduced in neocortex of DG cKO mice. Immunolabeling of synArfGEF showed clustered distribution and did not differ between genotypes. D, Overview

of S1 of DG cKO and control mice. Typical punctate CB1 immunofluorescence was lost across all layers of the cortex in DG cKO mice. E-I, Quantification of presynaptic GABAergic markers in S1 layer 2/3. VGAT and PV, and in contrast to hippocampus, also VGluT3 were not reduced in density and size in mice lacking neuronal DG (E, F, G). However, CB1 and CCK8 showed a similar reduction as in hippocampus in DG cKO mice compared to control mice (H and I). Data points represent individual mice. **p<0.01, ***p<0.001 (see Table 2 for statistical tests).

Figure 6. Neuronal dystroglycan is not necessary for clustering of glutamatergic synaptic proteins. A and B, To assess integrity of glutamatergic postsynaptic structures, antibodies to PSD-95 and bassoon were used and immunofluorescence quantified in stratum pyramidale and stratum radiatum. Cluster density and size was analyzed in stratum pyramidale and fluorescence intensity in stratum radiatum. All parameters analyzed did not differ between genotypes. C, VGluT1 was used as a marker of glutamatergic presynaptic terminals and puncta density and size in stratum pyramidale was quantified. No changes in VGluT1 puncta density and size were found between genotypes. D, PSD-95 apposition to VGluT1 was examined in stratum pyramidale and represented as percent PSD-95 clusters apposed to VGluT1 puncta. The apposition of PSD-95 to VGluT1 did not differ between genotypes. Data points represent individual mice. *p<0.05, ***p<0.001 (see Table 2 for statistical tests).

Figure 7. CCK-positive terminals are not established in the absence of neuronal dystroglycan. A, Triple immunofluorescence labeling of DG cKO and control CA1 pyramidal layer at postnatal day 21. B and C, Quantification of puncta density and size reveals loss of VGluT3 puncta in DG cKO tissue to the same degree as in adult mice (B) but unchanged PV immunolabeling (C). Data points represent individual mice. ***p<0.001 (see Table 2 for statistical tests).

Figure 8. Maintenance of CCK-positive basket terminals requires dystroglycan. A, Overview of experimental design. Virus was stereotactically injected unilaterally into CA1 region in adult mice heterozygous or homozygous for loxP sites flanking *Dag1* gene. B, After 14 dpi, Cre recombinase immunolabeling as well as mCherry fluorescence was clearly visible in

742 pyramidal cell somata. C, Example of injection site at 28 dpi. Cre expression was mostly
743 restricted to CA1 pyramidal cell layer. VGluT3 and dystrophin or DG immunofluorescence
744 was analyzed in the same sections. D, In mice containing homozygously floxed *Dag1*, β-DG
745 immunostaining was markedly reduced in CA1 pyramidal layer at 28 dpi. Heterozygous mice
746 showed a moderate reduction in β-DG immunofluorescence. E-G, As observed for β-DG, Cre
747 expression lead to loss of dystrophin in homozygously floxed mice whereas only a slight
748 decrease was observed in heterzygous mice. Reduction of dystrophin labeling was similar at
749 28 dpi (E), 42 dpi (F) and 84 dpi (G). H-J, Representative example images and
750 quantifications of VGluT3 immunostaining in CA1 pyramidal layer at 28 dpi (H), 42 dpi (I) and
751 84 dpi (J). Ipsilateral VGluT3 size and density in homozygously floxed mice was significantly
752 reduced compared to both contralateral side and ipsilateral side of heterozygously floxed
753 mice. With increased time after injection this reduction of VGluT3 puncta became more
754 prominent. Data points represent individual mice. *p<0.05, **p<0.01, ***p<0.001 (see Table 2
755 for statistical tests).
756 Figure 9. Frequency and amplitude of sIPSCs are reduced in dystroglycan cKO pyramidal
757 cells. A, Image showing the position of the recording pipette in the hippocampal CA1 region
758 (left, 4x), and an example image of a typical CA1 pyramidal cell identified using LED
759 illumination (Alexa Fluor 488, right, 40x). B, Representative example traces of whole-cell
760 sIPSC recordings from control mice (left trace) and DG cKO mice (right trace). Average
761 sIPSCs are shown above the traces. C, Cumulative frequency plot of inter-event intervals of
762 sIPSCs from control (blue line) and DG cKO cell (red line) from the traces in B (left panel)
763 and cumulative frequency plot of sIPSC amplitudes from the same cells (right panel). D,
764 Comparison of average sIPSC frequency and amplitude between control and DG cKO slices.
765 DG cKO mice exhibit significantly lower sIPSC frequency and amplitude than control mice.
766 Data points represent individual cells. *p<0.05.
767 Figure 10. Dystroglycan is necessary for carbachol-induced increase of inhibitory currents in
768 pyramidal cells. A, Representative example traces of sIPSC recordings before (baseline, left
769 trace) and after the application of carbachol (CCh, right trace) in control mice. Average

sIPSCs are shown above the traces. B, Cumulative frequency plots of inter-event intervals (IEI) and amplitudes of sIPSCs from traces in A. C, Comparison of average sIPSC frequency and amplitude before and after application of CCh in control slices. Application of CCh resulted in typical increase of IPSC frequency in control pyramidal cells but amplitude was not affected by CCh. D, Representative example traces of sIPSC recordings before (baseline, left trace) and after the application of CCh (right trace) in DG cKO mice. Average sIPSCs are shown above the traces. E, Cumulative frequency plots of inter-event intervals (IEI) and amplitudes of sIPCSs from traces in D. F, Comparison of average sIPSC frequency and amplitude before and after application of CCh in DG cKO slices. In contrast to control slices, application of CCh did not lead to a significant increase of sIPSC frequency in DG cKO pyramidal cells. Data points represent individual cells. **p<0.01.

Figure 11. Neurexin- and laminin-binding of α-dystroglycan is not essential for formation of CCK-positive basket terminals on pyramidal cells. A and B, Triple immunofluorescence labeling of GABAergic markers in CA1 pyramidal layer of *Dag1* T190M and wildtype mice. A, Antibody to β-DG revealed typical clustered distribution in *Dag1* T190M mice. VGluT3 and PV immunofluorescence was indistinguishable between genotypes. B, Intensity of DG clusters was markedly reduced and background staining increased using the α-DG glycosylation-specific antibody 11H6, confirming glycosylation deficits of synaptic DG in T190M mice. CB1 and $GABA_AR$ γ2 subunit immunofluorescence was indistinguishable between genotypes. C and D, Quantification of density and size of VGluT3 (C) and CB1 (D) puncta in CA1 pyramidal layer of *Dag1* T190M and wildtype mice. Density and size of puncta did not differ significantly between genotypes. E, Quantification of β-DG apposition to PV and/or VGluT3 in CA1 pyramidal layer. Data represent number of β-DG clusters apposed to PV or VGluT3 or both (triple colocalized) as percentage of total β-DG clusters. Apposition of β-DG to presynaptic markers did not differ significantly between genotypes. Data points represent individual mice. See Table 2 for statistical tests.

Illustrations and Tables

Table 1. Antibodies used for immunohistochemical stainings

Target	Host species	Dilution	Cat. no.	Company / origin
α-Dystroglycan (VIA4-1)	Mouse	1:100	05-298	EMD Millipore
α-Dystroglycan (11H6C4)	Mouse	1:100	05-593	EMD Millipore
β-Dystroglycan	Mouse	1:100	ab49515	Abcam
Bassoon	Mouse	1:2000	VAM-PS003	StressGen
Cannabinoid receptor 1	Rabbit	1:3000	258 003	Synaptic Systems
Cholecystokinin 8	Mouse	1:1000	ab37274	Abcam
Cre recombinase	Rabbit	1:1000	PRB-106C	Covance
Dystrophin (C-terminal)	Mouse	1:100	BT39-9050-05	Biotrend
$GABA_AR$ α1 subunit	Guinea pig	1:20‘000	-	(Fritschy and Mohler, 1995)
$GABA_AR$ α2 subunit	Guinea pig	1:6000	-	(Fritschy and Mohler, 1995)
$GABA_AR$ γ2 subunit	Guinea pig	1:10‘000	-	(Fritschy and Mohler, 1995)
GAD65/67	Rabbit	1:2000	GC 3008	Biomol
Gephyrin	Mouse	1:1000	147 021	Synaptic Systems
NeuN	Mouse	1:1000	MAB377	Chemicon
Neuroligin 2	Rabbit	1:10‘000	-	Gift from Dr. Peter Scheiffele
Parvalbumin	Rabbit	1:1000	24428	ImmunoStar
PSD-95	Mouse	1:1000	MA1-045	ABR
Synaptotagmin 2	Rabbit	1:1000	105 123	Synaptic Systems
synArfGEF	Guinea pig	1:3000	-	Gift from Dr. Hiroyuki Sakagami (Fukaya et al., 2011)
VGAT	Rabbit	1:3000	131 003	Synaptic Systems
VGluT1	Guinea pig	1:1000	135 304	Synaptic Systems
VGluT3	Guinea pig	1:4000	AB5421	Merck Millipore

Table 1. Antibodies used for immunohistochemical stainings. If not otherwise stated, antibody VIA4-1 was used to label α-dystroglycan. For secondary antibodies see Materials and Methods.

803 **Table 2. Results of statistical tests performed for immunohistochemical stainings**

Epitope	Conditions	Unpaired t-test (density)	Kolmogorov-Smirnov test (size)
$GABA_AR$ α1 subunit	DG cKO / adult / CA1	t_6=0.920, p=0.393	n=33385, D=12.662, p<0.001
$GABA_AR$ α2 subunit	DG cKO / adult / CA1	t_{15}=3.816, p=0.002	n=18495, D=3.484, p<0.001
$GABA_AR$ γ2 subunit	DG cKO / adult / CA1	t_7=1.607, p=0.152	n=31807, D=3.692, p<0.001
Gephyrin	DG cKO / adult / CA1	t_7=1.252, p=0.251	n=39289, D=0.720, p=0.677
Neuroligin 2	DG cKO / adult / CA1	t_6=0.979, p=0.366	n=32217, D=5.476, p<0.001
synArfGEF	DG cKO / adult / CA1	t_6=1.093, p=0.316	n=22737, D=3.850, p<0.001
VGAT	DG cKO / adult / CA1	t_{15}=0.646, p=0.528	n=20569, D=0.528, p=0.943
	DG cKO / adult / neocortex	t_9=1.309, p=0.223	n=24713, D=1.107, p=0.172
Parvalbumin	DG cKO / adult / CA1	t_7=0.198, p=0.849	n=24929, D=1.068, p=0.204
	DG cKO / adult / neocortex	t_9=0.454, p=0.661	n=20534, D=4.845, p<0.001
	DG cKO / P21 / CA1	t_8=0.869, p=0.410	n=8010, D=1.037, p=0.233
Cannabinoid receptor 1	DG cKO / adult / CA1	t_6=16.869, p<0.001	n=4654, D=4.325, p<0.001
	DG cKO / adult / neocortex	t_{11}=7.117, p<0.001	n=8067, D=6.960, p<0.001
	T190M / adult / CA1	t_8=0.681, p=0.515	n=9152, D=0.881, p=0.420
Synaptotagmin 2	DG cKO / adult / CA1	t_9=1.456, p=0.179	n=3397, D=1.977, p=0.001
Cholecystokinin 8	DG cKO / adult / CA1	t_{17}=6.292, p<0.001	n=5111, D=4.133, p<0.001
	DG cKO / adult / neocortex	t_6=4.475, p=0.004	n=1387, D=1.874, p=0.002
PSD-95	DG cKO / adult / CA1 / SP	t_6=1.106, p=0.311	n=16281, D=1.554, p=0.016
	DG cKO / adult / CA1 / SR	t_6=0.243, p=0.817	-
Bassoon	DG cKO / adult / CA1 / SP	t_{10}=0.767, p=0.461	n=32489, D=2.275, p<0.001
	DG cKO / adult / CA1 / SR	t_{10}=0.871, p=0.404	-
VGluT1	DG cKO / adult / CA1	t_6=0.094, p=0.928	n=12776, D=0.492, p=0.969
VGluT3	DG cKO / adult / CA1	t_{21}=13.213, p<0.001	n=5975, D=8.273, p<0.001
	DG cKO / adult / neocortex	t_9=0.456, p=0.659	n=6523, D=2.054, p<0.001
	DG cKO / P21 / CA1	t_8=13.437, p<0.001	n=1830, D=8.270, p<0.001
	T190M / adult / CA1	t_8=0.494, p=0.634	n=4763, D=0.702, p=0.708

		t-test (unpaired between genotypes, paired between	Kruskal-	Dunn's multiple

Conditions	hemispheres; density)	Wallis test (size)	comparison test (size)
28dpi / loxP/+	t_3=0.520, p=0.639	n=13610	y=283.498, p<0.05
28dpi / loxP/loxP	t_4=2.895, p=0.044	H=55.796	y=539.294, p<0.001
28dpi / contralateral	t_7=1.032, p=0.336	p<0.001	y=136.188, p>0.05
28dpi / ipsilateral	t_7=2.894, p=0.023		y=391.984, p<0.001
42dpi / loxP/+	t_4=0.870, p=0.434	n=9915	y=93.906, p>0.05
42dpi / loxP/loxP	t_4=3.478, p=0.025	H=87.162	y=693.091, p<0.001
42dpi / contralateral	t_8=1.040, p=0.329	p<0.001	y=82.049, p>0.05
42dpi / ipsilateral	t_8=4.059, p=0.004		y=681.234, p<0.001
84dpi / loxP/+	t_5=1.843, p=0.125	n=7378	y=16.550, p>0.05
84dpi / loxP/loxP	t_3=8.578, p=0.003	H=52.415	y=466.868, p<0.001
84dpi / contralateral	t_8=0.682, p=0.515	P<0.001	y=143.428, p>0.05
84dpi / ipsilateral	t_8=3.495, p=0.008		y=593.745, p<0.001

Table 2. Results of statistical tests performed for immunohistochemical stainings. Numbers in subscript in t-tests represent degrees of freedom. D, H and y represent test statistics for Kolmogorov-Smirnov tests, Kruskal-Wallis tests and Dunn's multiple comparison tests, respectively.

Figure 1

A

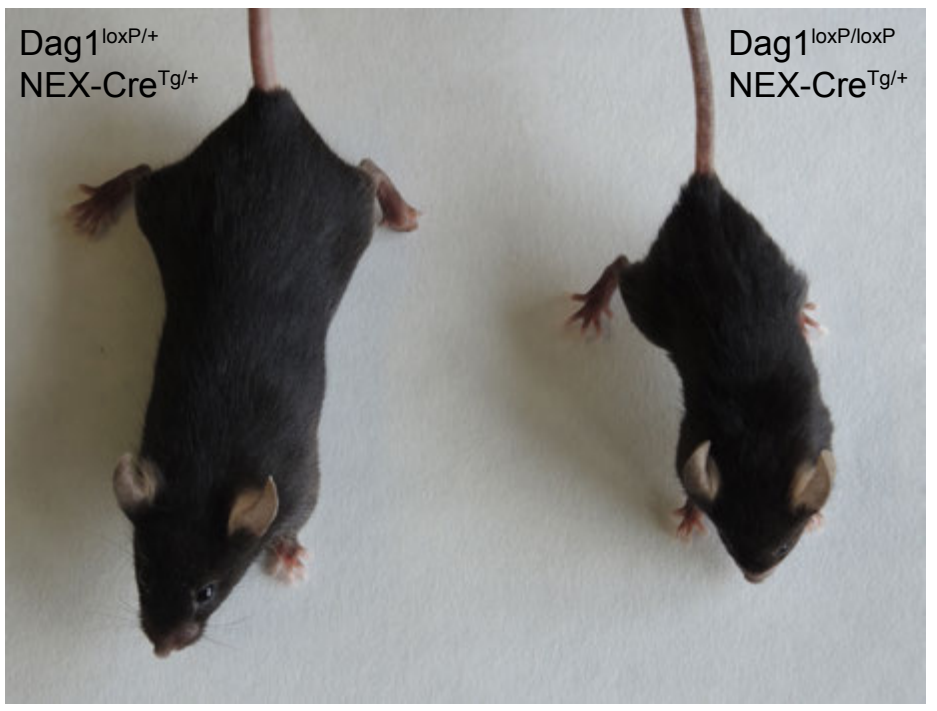

B

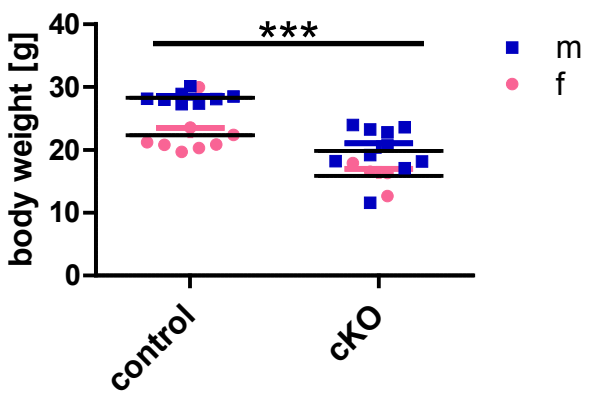

C

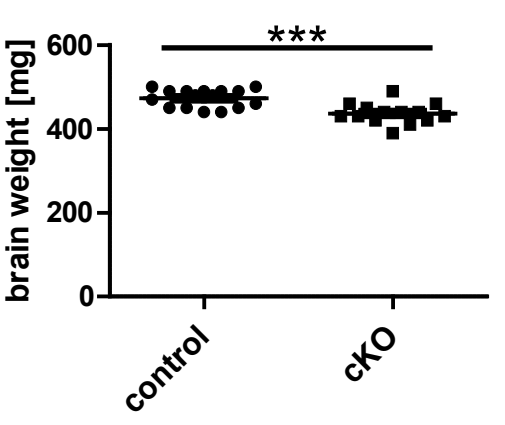

D

Mice at 2.5 months of age:

NEX-Cre$^{tg/+}$ Dag1$^{loxP/+}$	NEX-Cre$^{tg/+}$ Dag1$^{loxP/loxP}$
27 (25.2%)	19 (17.8%)

E

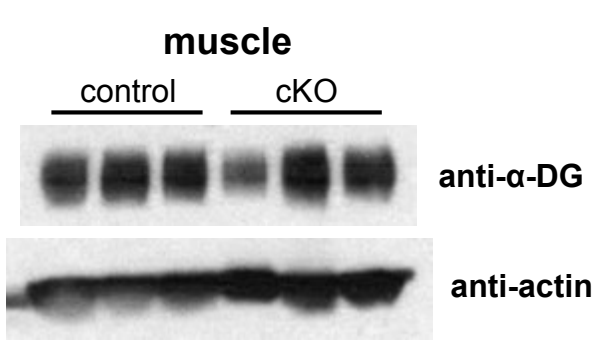

F

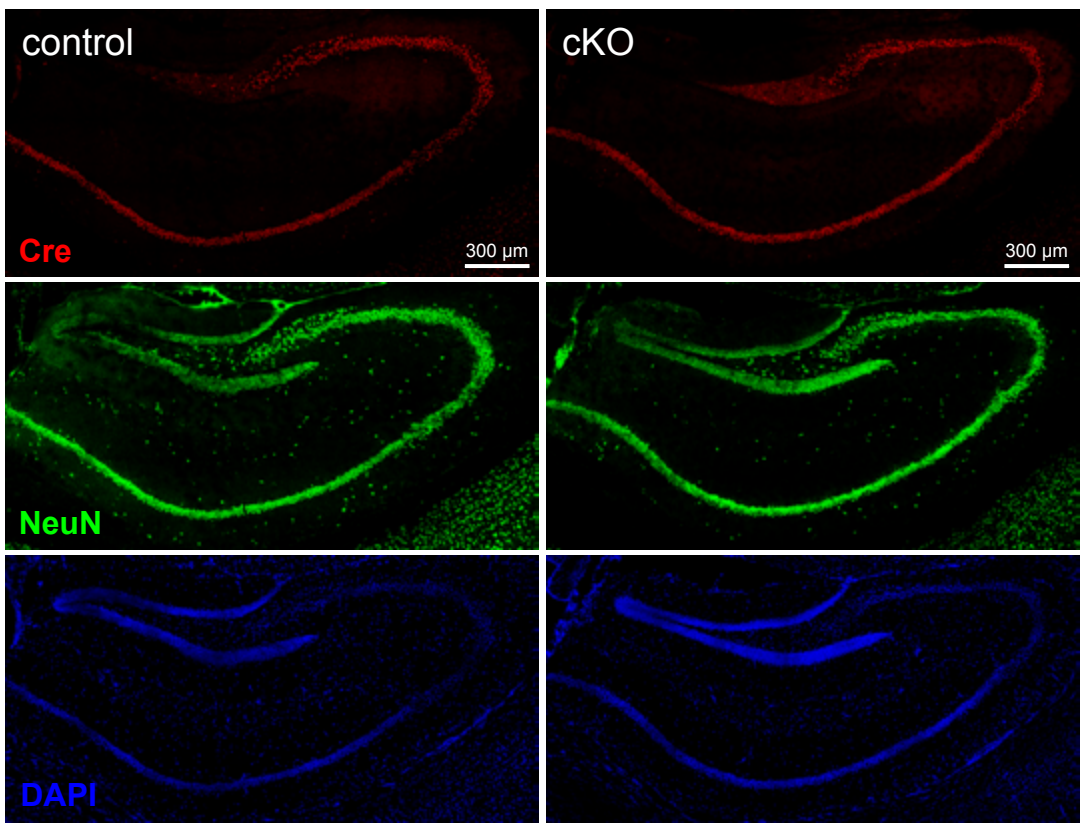

G

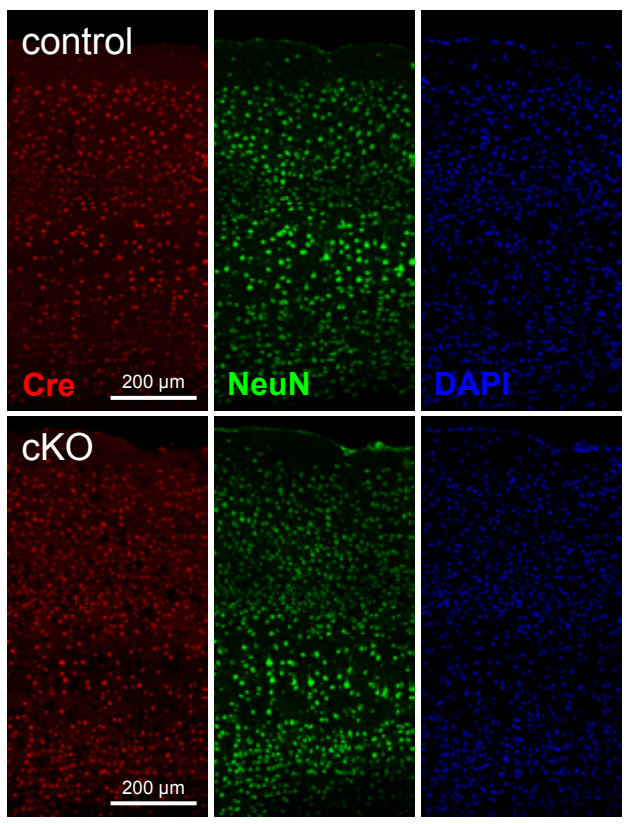

Figure 2

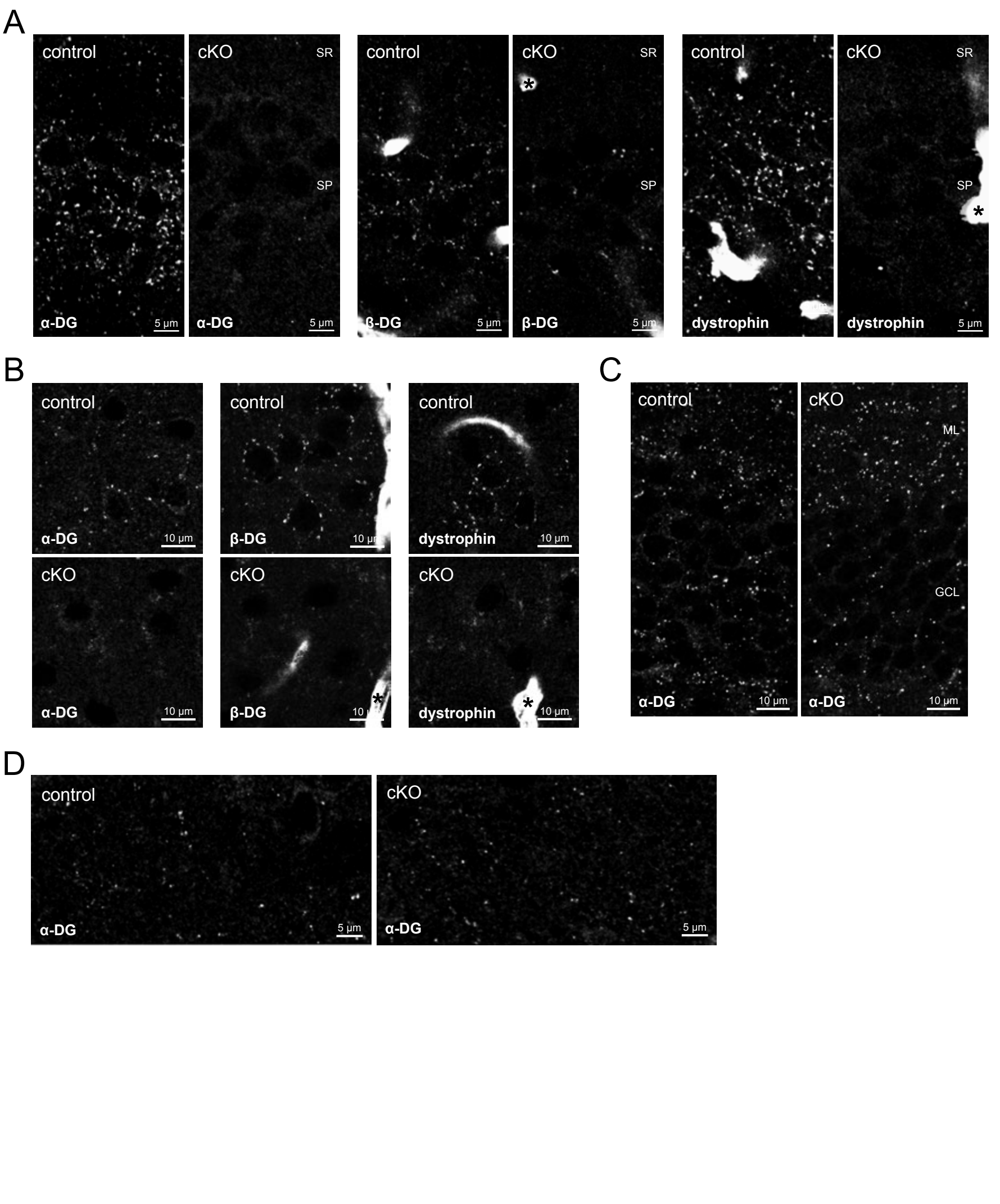

Figure 3

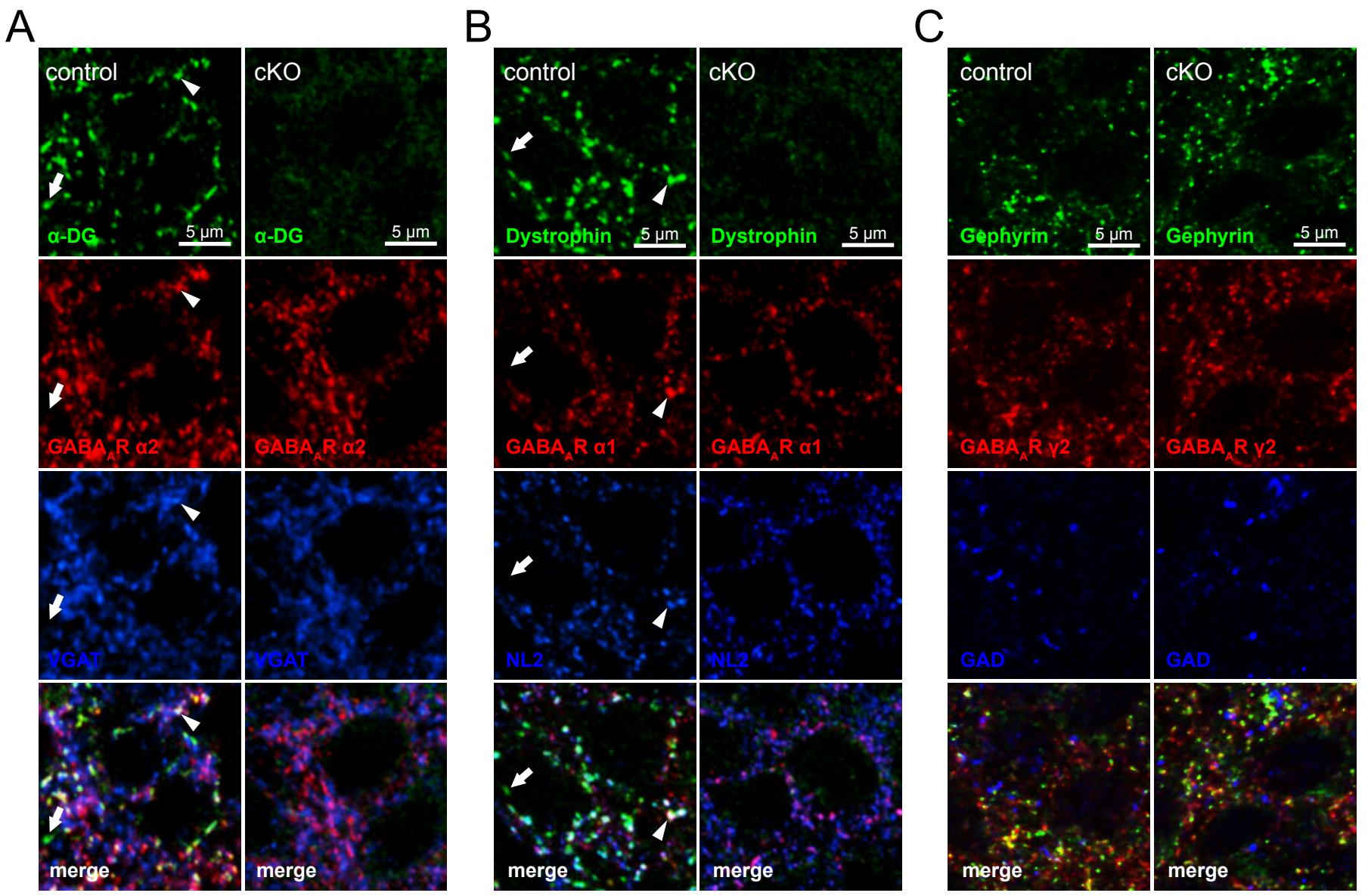
A
control
cKO
α-DG
5 µm
GABA$_A$R α2
VGAT
merge
B
Dystrophin
GABA$_A$R α1
NL2
C
Gephyrin
GABA$_A$R γ2
GAD

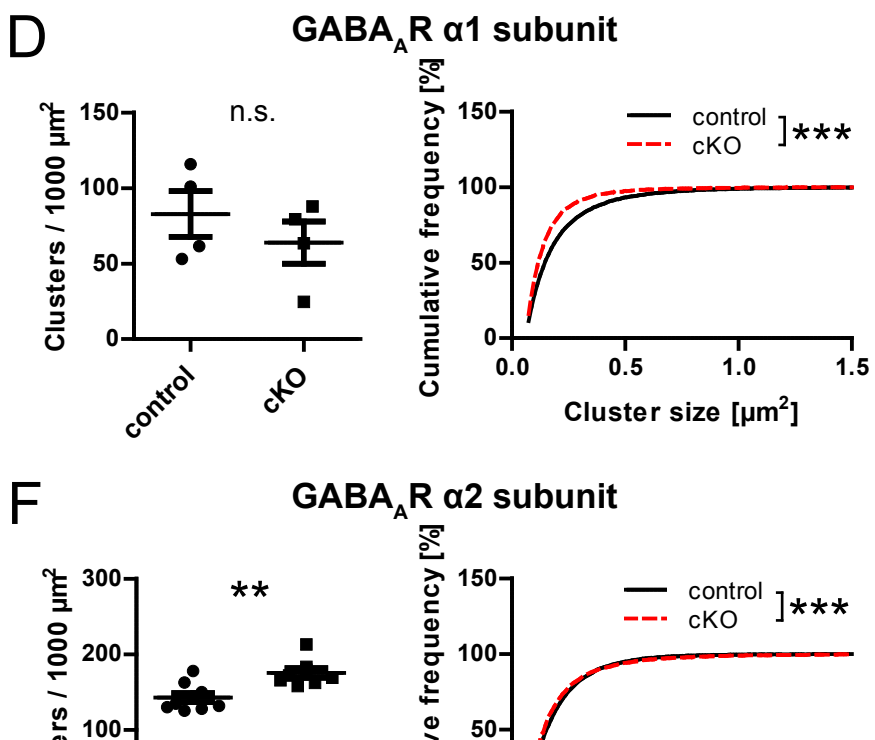
D
GABA$_A$R α1 subunit
Clusters / 1000 µm^2
n.s.
control
cKO
Cumulative frequency [%]
***
Cluster size [µm^2]

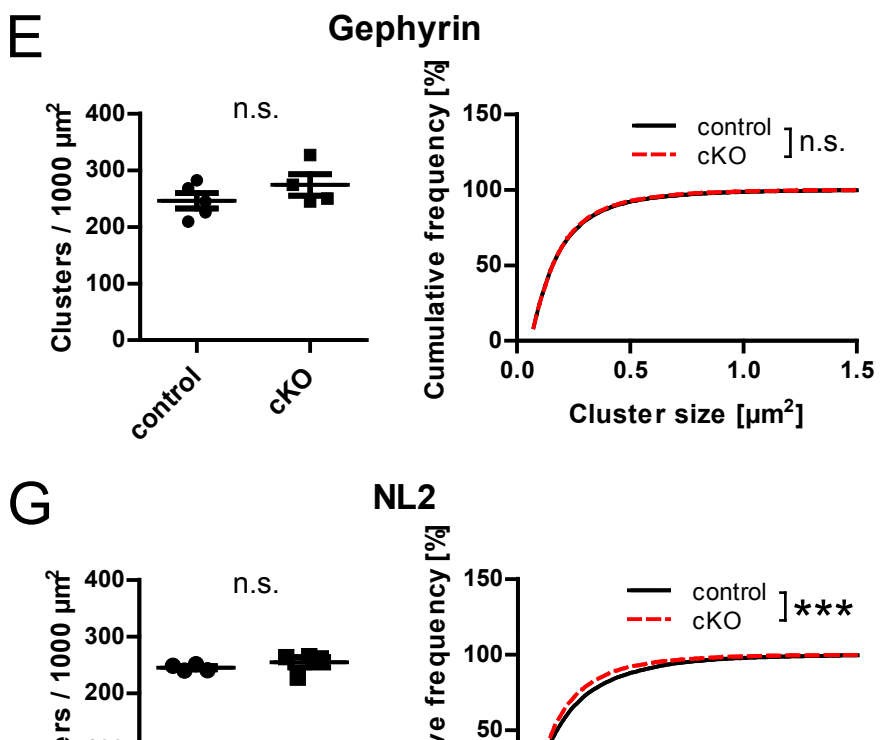
E
Gephyrin
n.s.

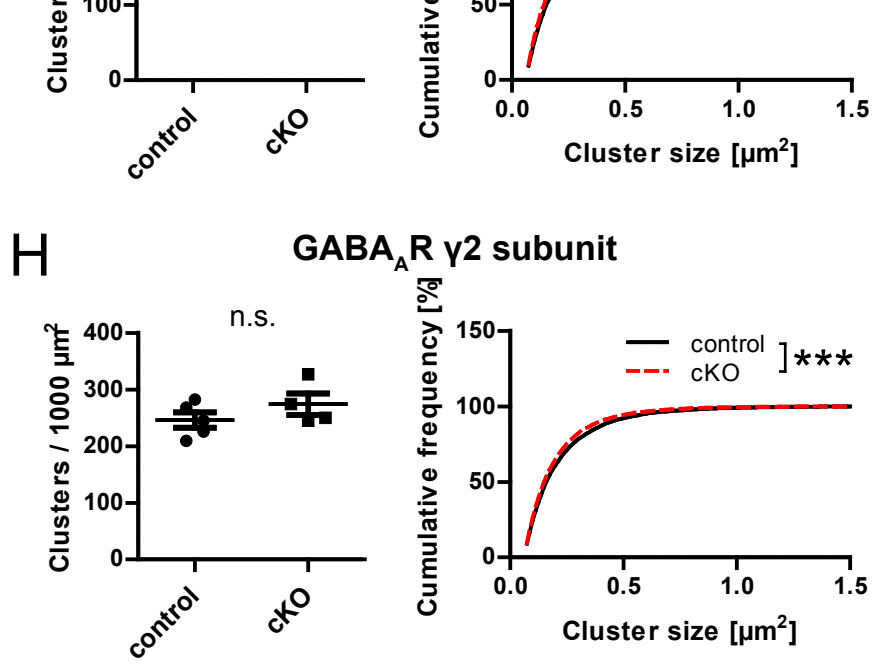
F
GABA$_A$R α2 subunit
**
***

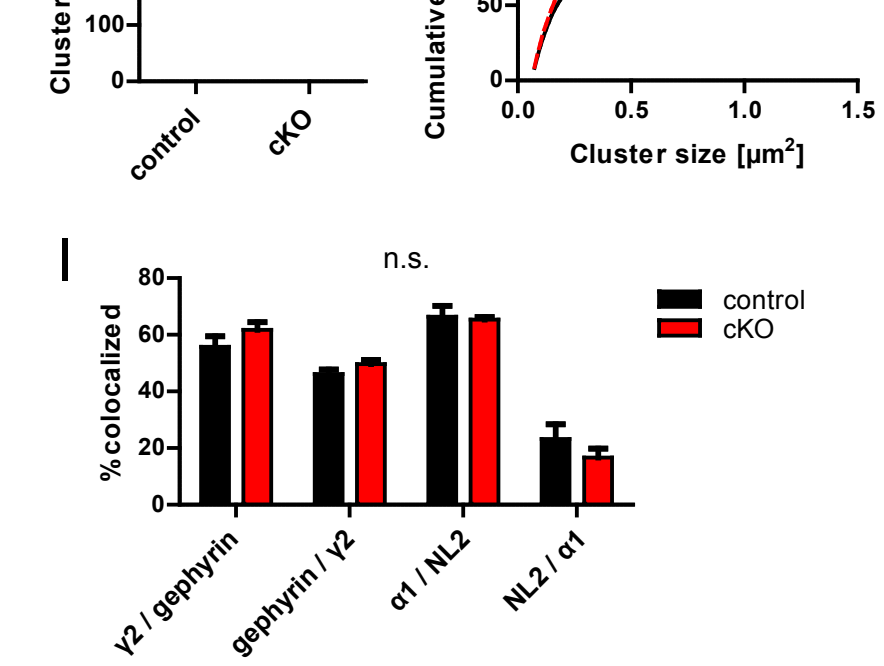
G
NL2
n.s.
***

H
GABA$_A$R γ2 subunit
n.s.
***

I
n.s.
control
cKO
% colocalized
γ2 / gephyrin
gephyrin / γ2
α1 / NL2
NL2 / α1

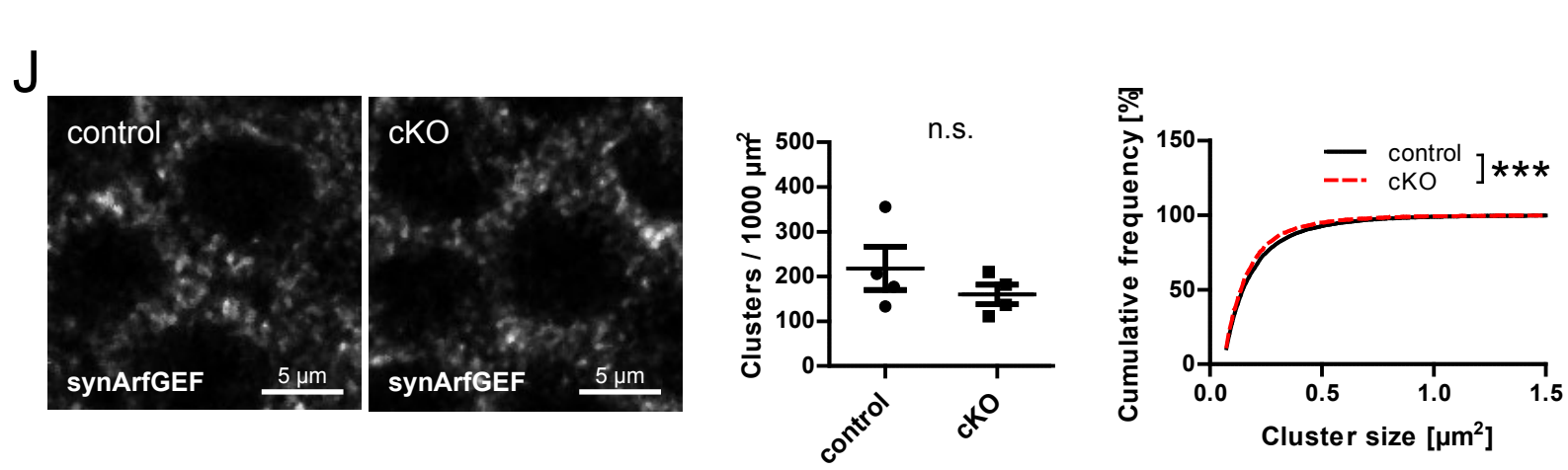
J
control
cKO
synArfGEF
5 µm
n.s.
***

Figure 4

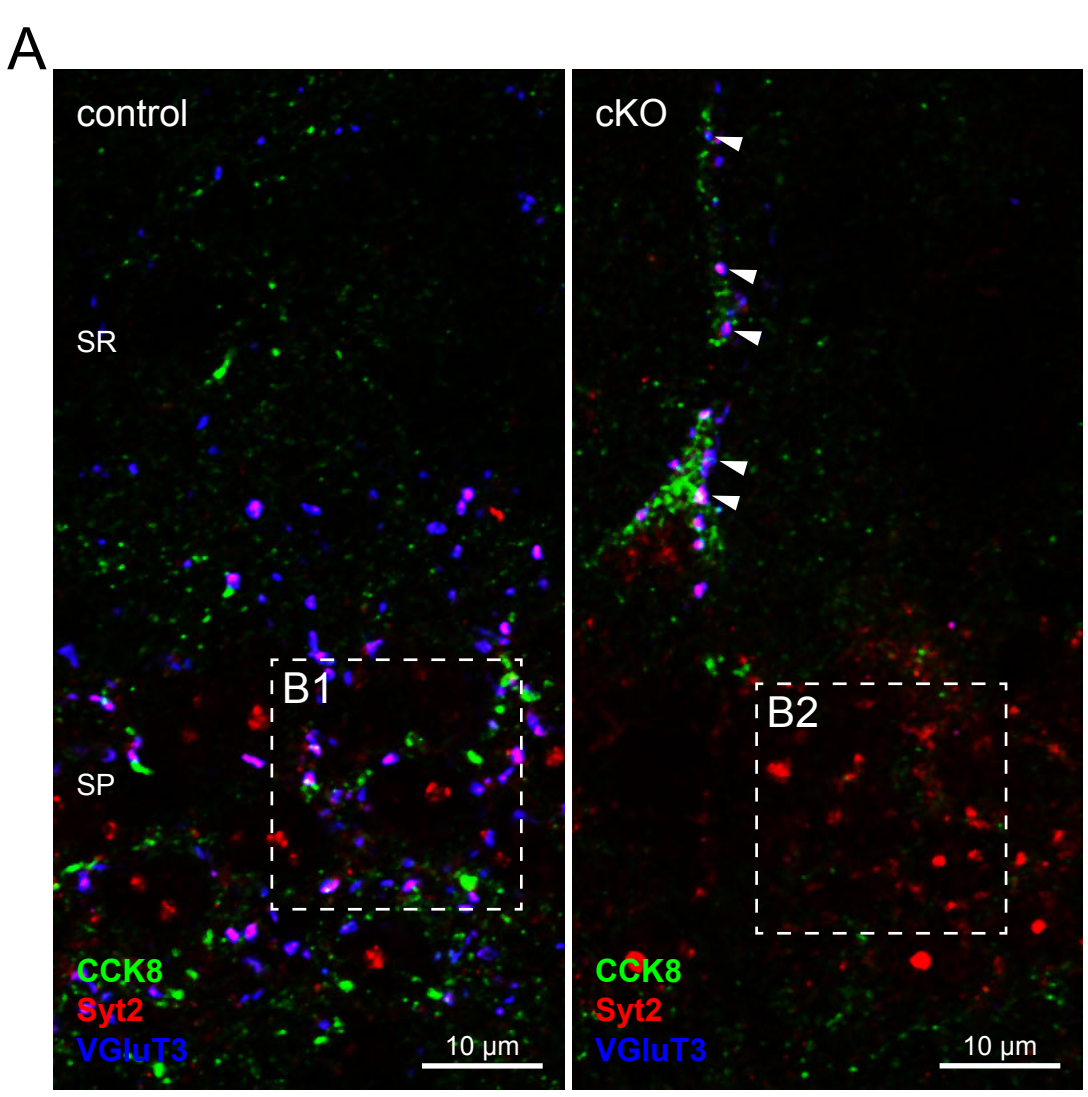
A
control
cKO
SR
SP
B1
B2
CCK8
Syt2
VGluT3
10 μm

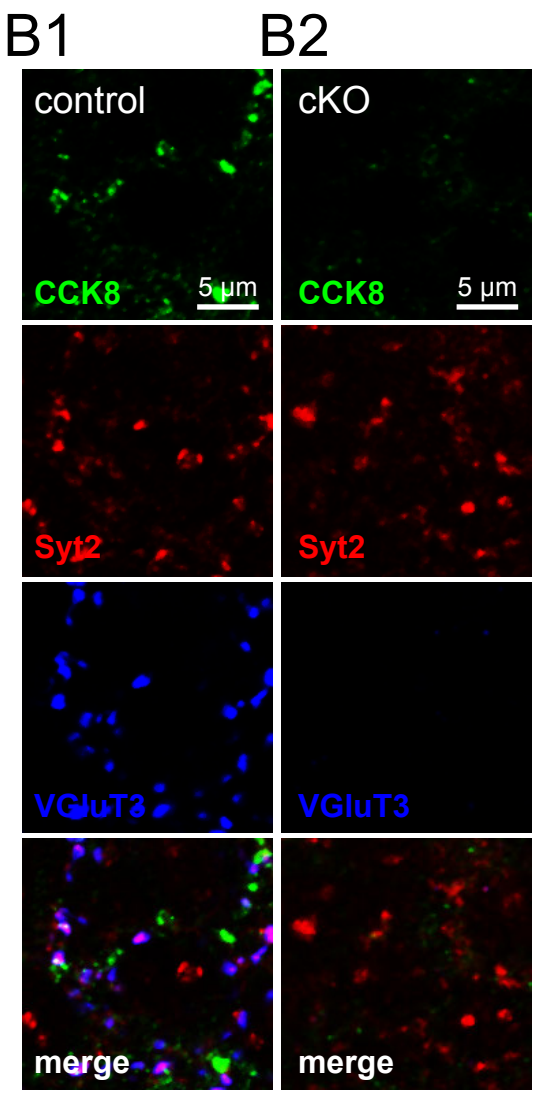
B1
B2
control
cKO
CCK8
Syt2
VGluT3
merge
5 μm

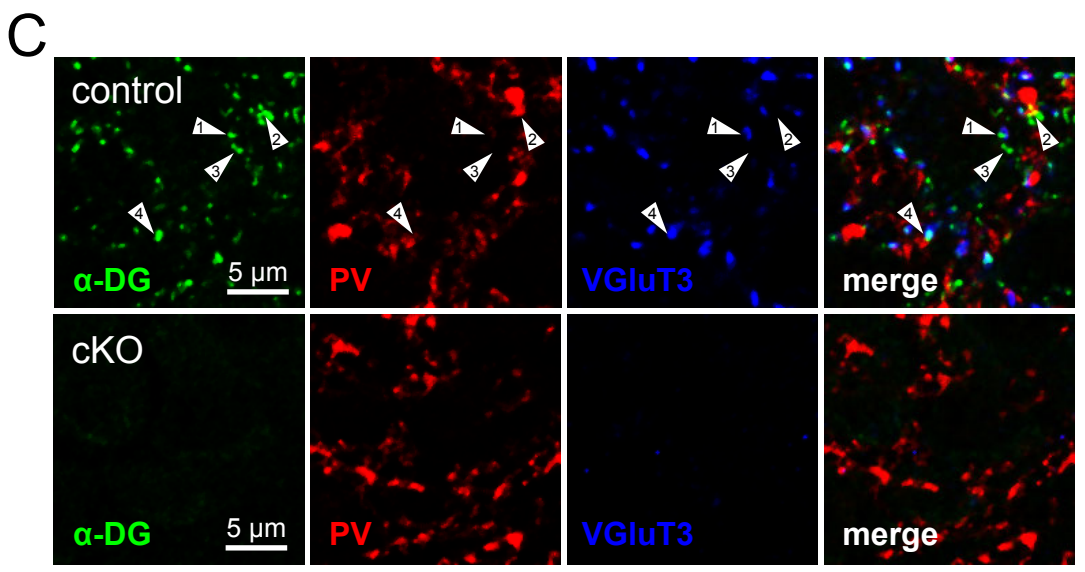
C
control
cKO
α-DG
PV
VGluT3
merge
5 μm

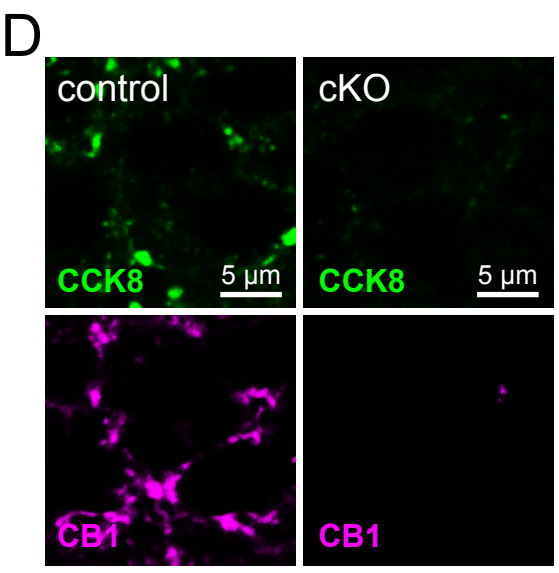
D
control
cKO
CCK8
CB1
merge
5 μm

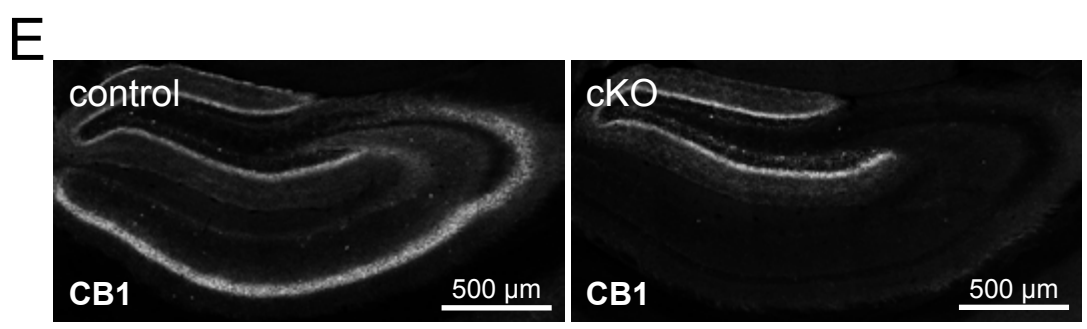
E
control
cKO
CB1
500 μm

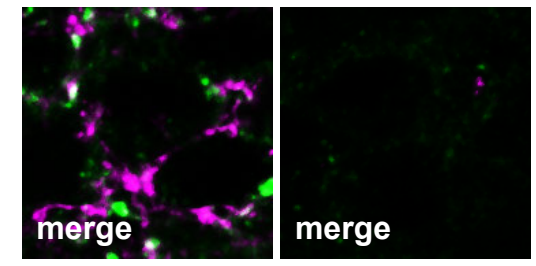
merge

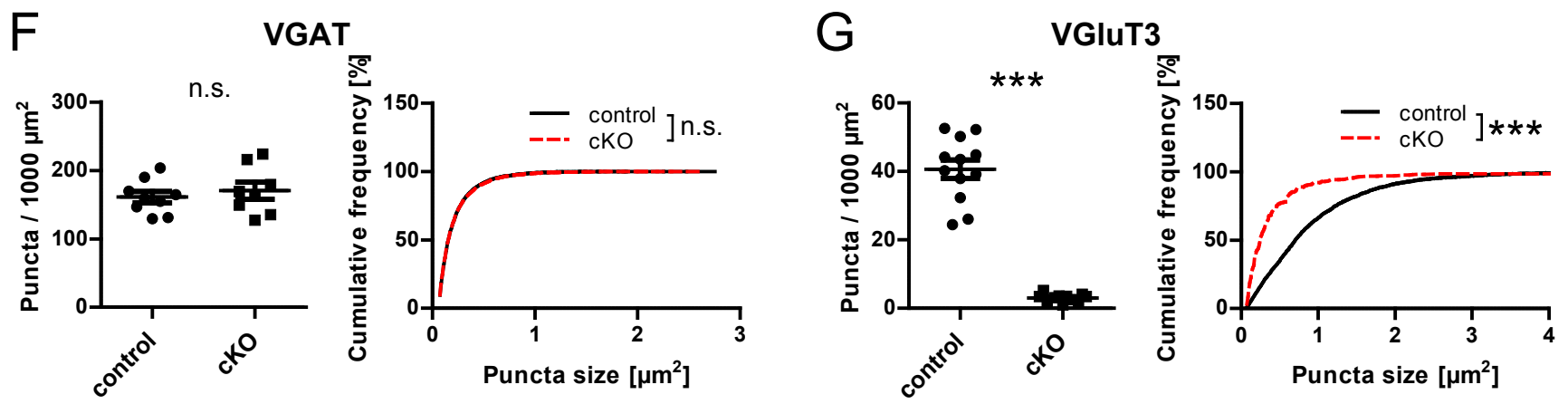
F
VGAT
n.s.
Puncta / 1000 μm²
control
cKO
Cumulative frequency [%]
Puncta size [μm²]
G
VGluT3
***

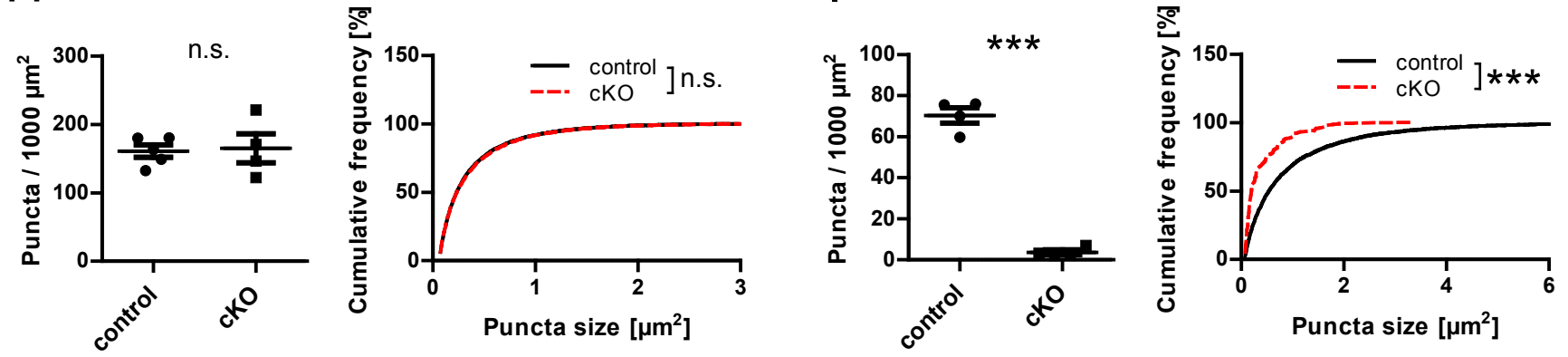
H
PV
n.s.
I
CB1
***

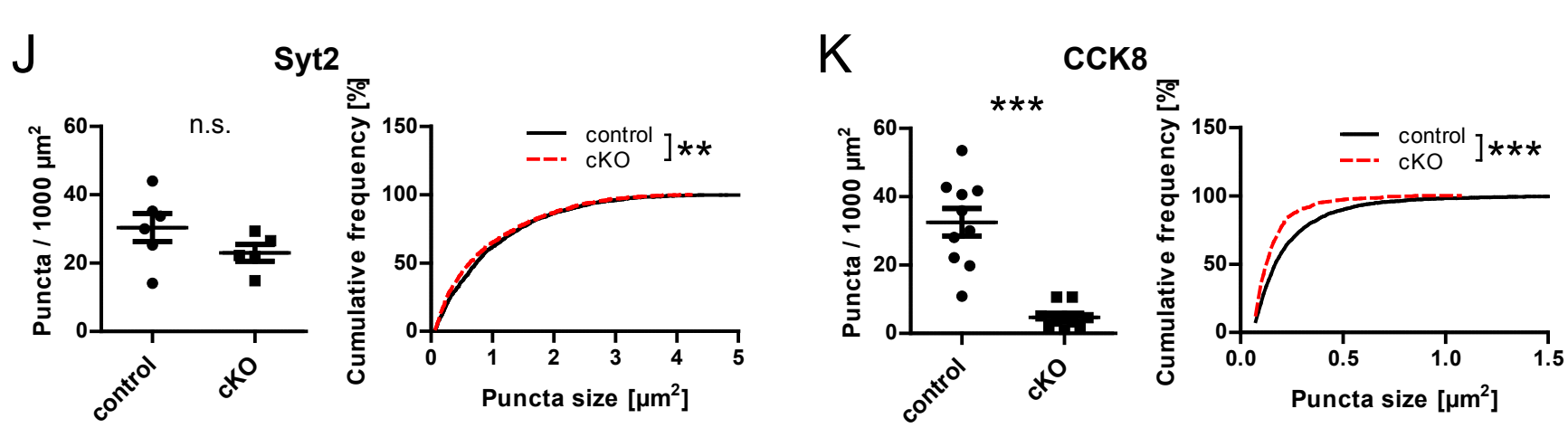
J
Syt2
n.s.
**
K
CCK8
***

Figure 5

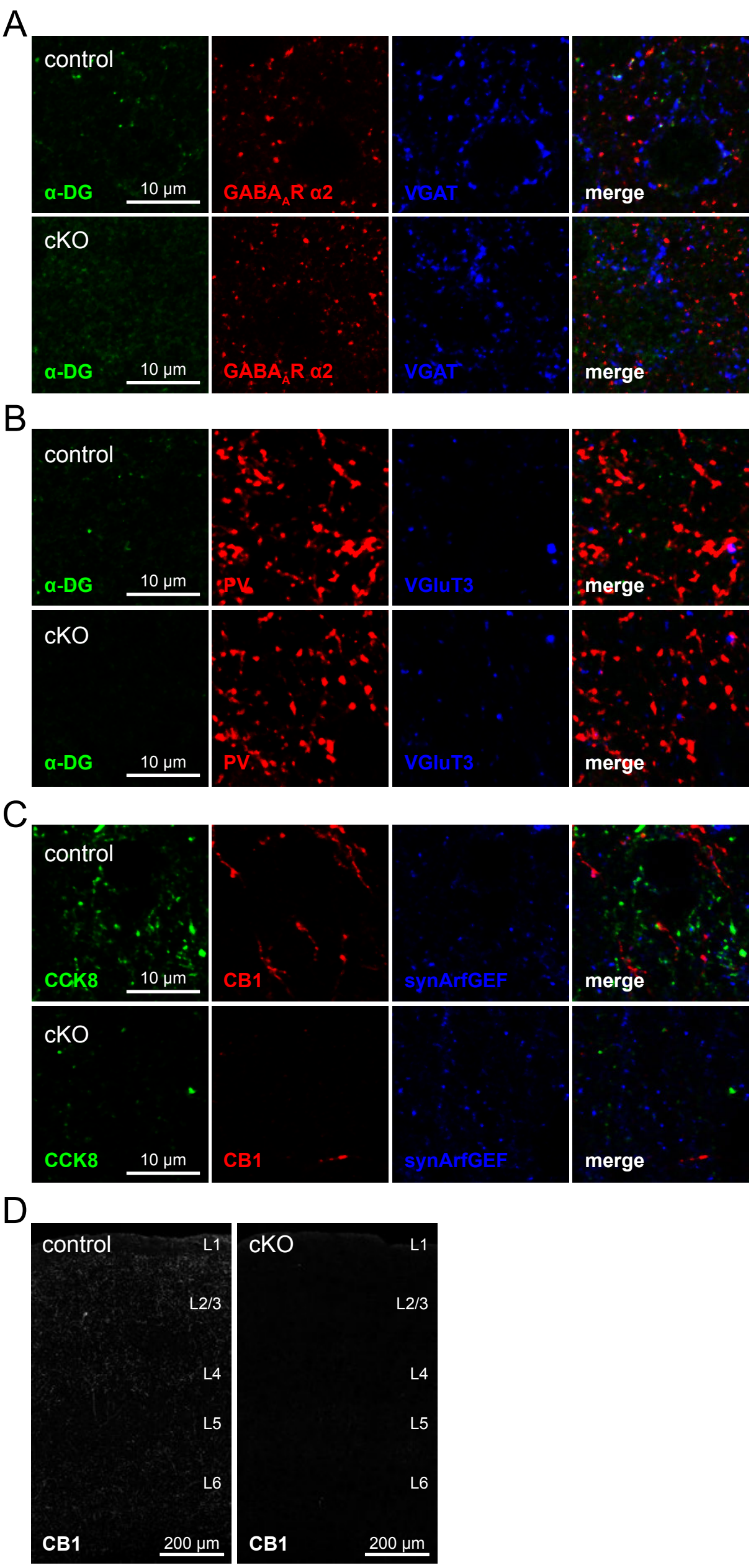
A
control
α-DG
10 µm
GABA$_A$R α2
VGAT
merge
cKO
α-DG
10 µm
GABA$_A$R α2
VGAT
merge
B
control
α-DG
10 µm
PV
VGluT3
merge
cKO
α-DG
10 µm
PV
VGluT3
merge
C
control
CCK8
10 µm
CB1
synArfGEF
merge
cKO
CCK8
10 µm
CB1
synArfGEF
merge
D
control
L1
L2/3
L4
L5
L6
CB1
200 µm
cKO
L1
L2/3
L4
L5
L6
CB1
200 µm

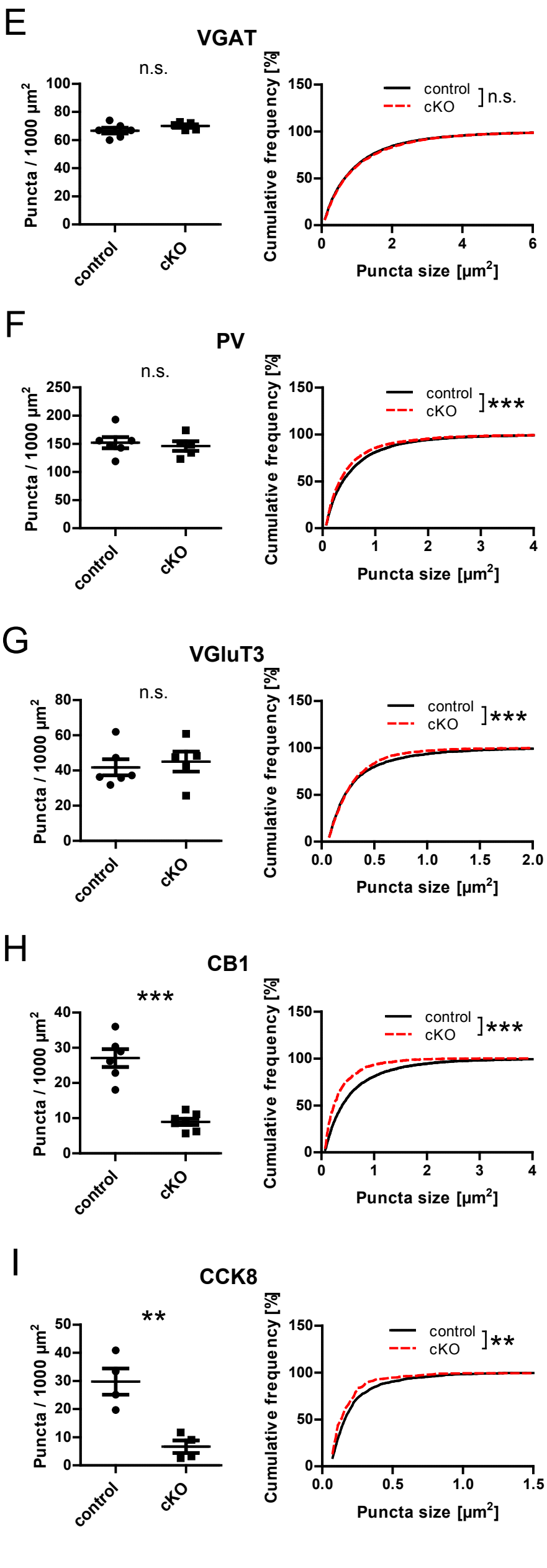
E
VGAT
n.s.
Puncta / 1000 µm^2
control
cKO
Cumulative frequency [%]
control
cKO
n.s.
Puncta size [µm^2]
F
PV
n.s.
Puncta / 1000 µm^2
control
cKO
Cumulative frequency [%]
control
cKO
***
Puncta size [µm^2]
G
VGluT3
n.s.
Puncta / 1000 µm^2
control
cKO
Cumulative frequency [%]
control
cKO
***
Puncta size [µm^2]
H
CB1
***
Puncta / 1000 µm^2
control
cKO
Cumulative frequency [%]
control
cKO
***
Puncta size [µm^2]
I
CCK8
**
Puncta / 1000 µm^2
control
cKO
Cumulative frequency [%]
control
cKO
**
Puncta size [µm^2]

Figure 6

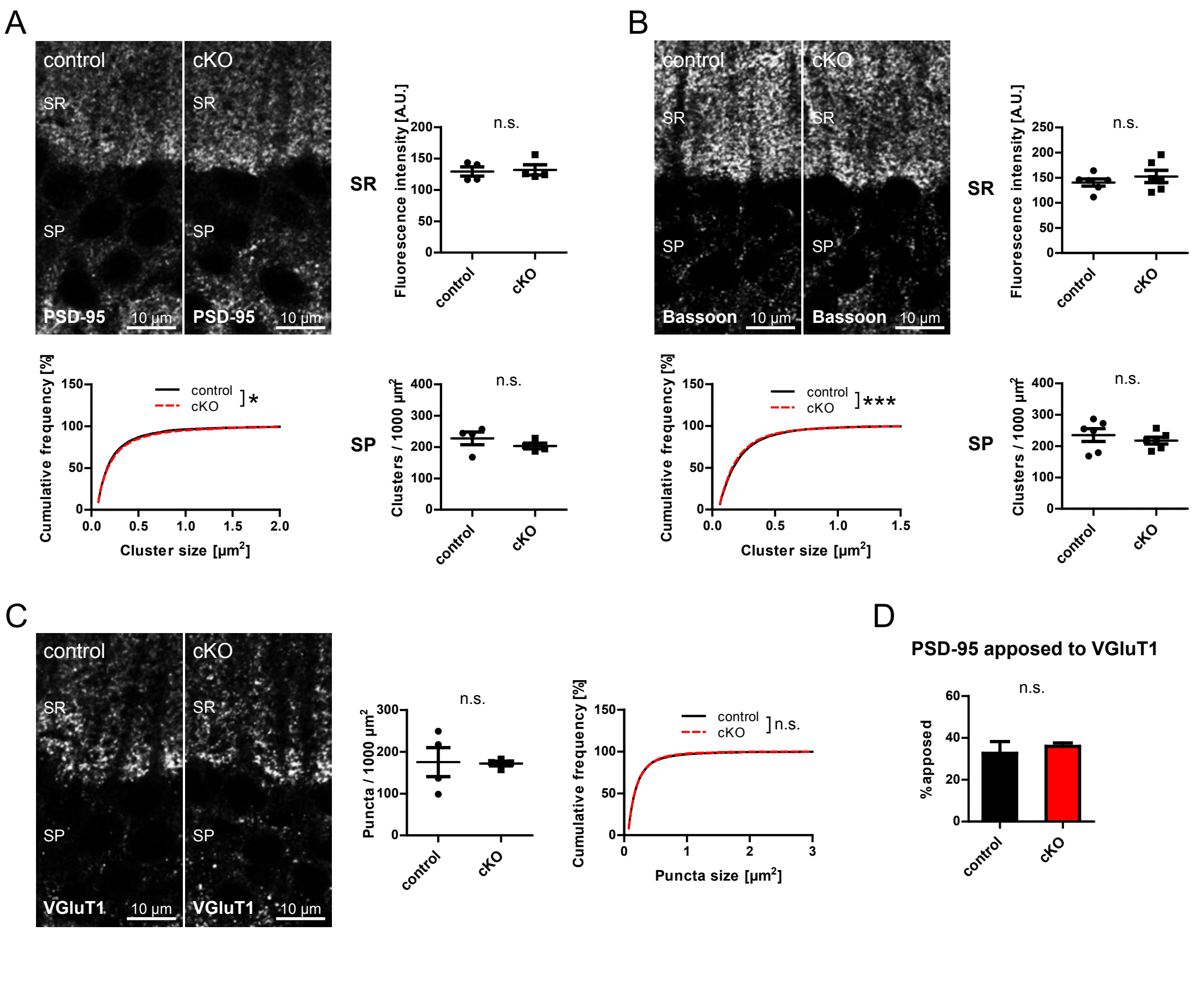
A
control
cKO
SR
SP
PSD-95
10 µm
Fluorescence intensity [A.U.]
n.s.
SR
control
cKO
Cumulative frequency [%]
]*
Cluster size [µm²]
Clusters / 1000 µm²
SP
B
Bassoon
]***
C
VGluT1
Puncta / 1000 µm²
]n.s.
Puncta size [µm²]
D
PSD-95 apposed to VGluT1
% apposed

Figure 7

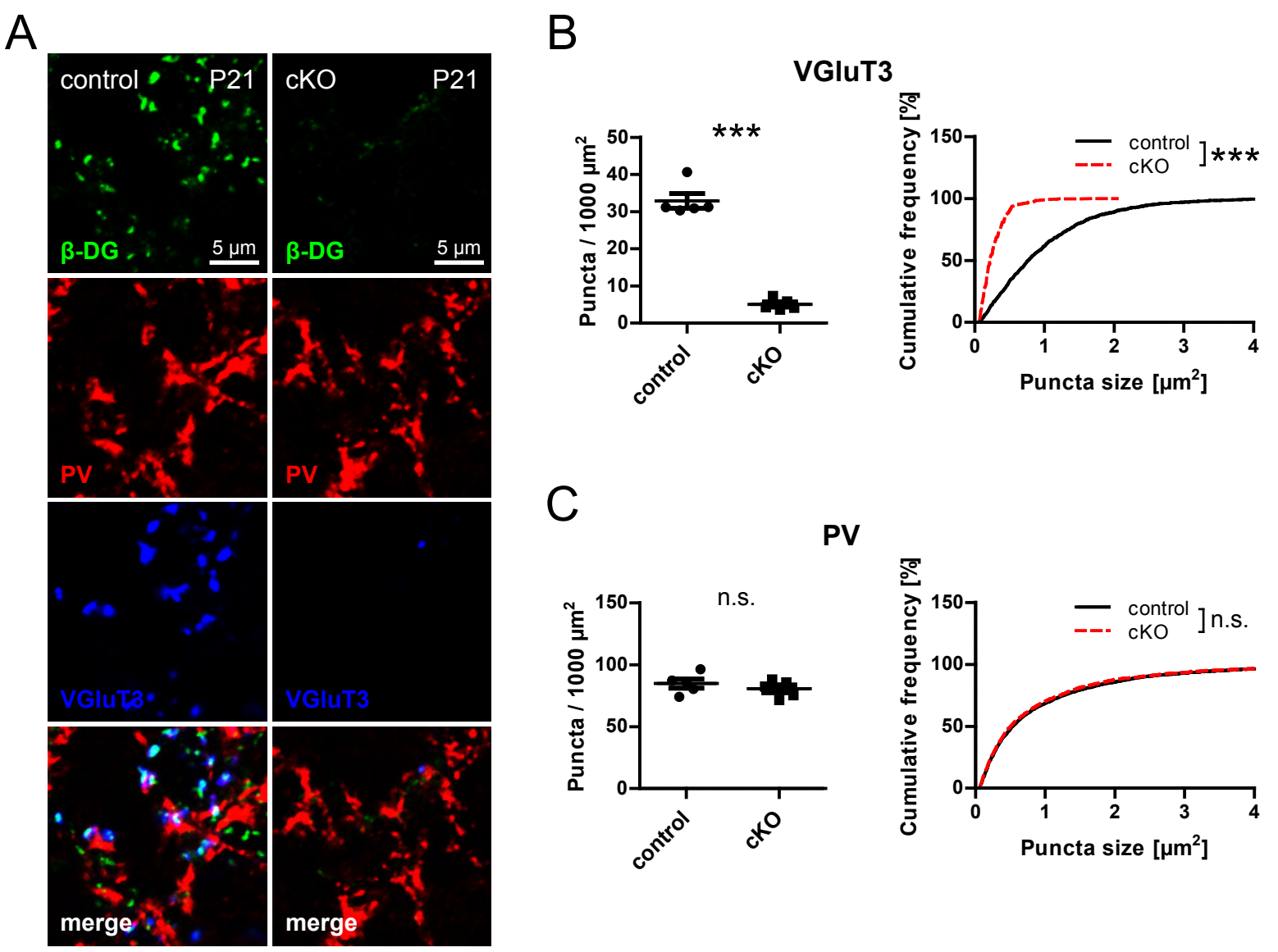
A
control
P21
cKO
P21
β-DG
5 µm
β-DG
5 µm
PV
PV
VGluT3
VGluT3
merge
merge
B
VGluT3
Puncta / 1000 µm²
***
control
cKO
Cumulative frequency [%]
control
cKO
]***
Puncta size [µm²]
C
PV
Puncta / 1000 µm²
n.s.
control
cKO
Cumulative frequency [%]
control
cKO
]n.s.
Puncta size [µm²]

Figure 8

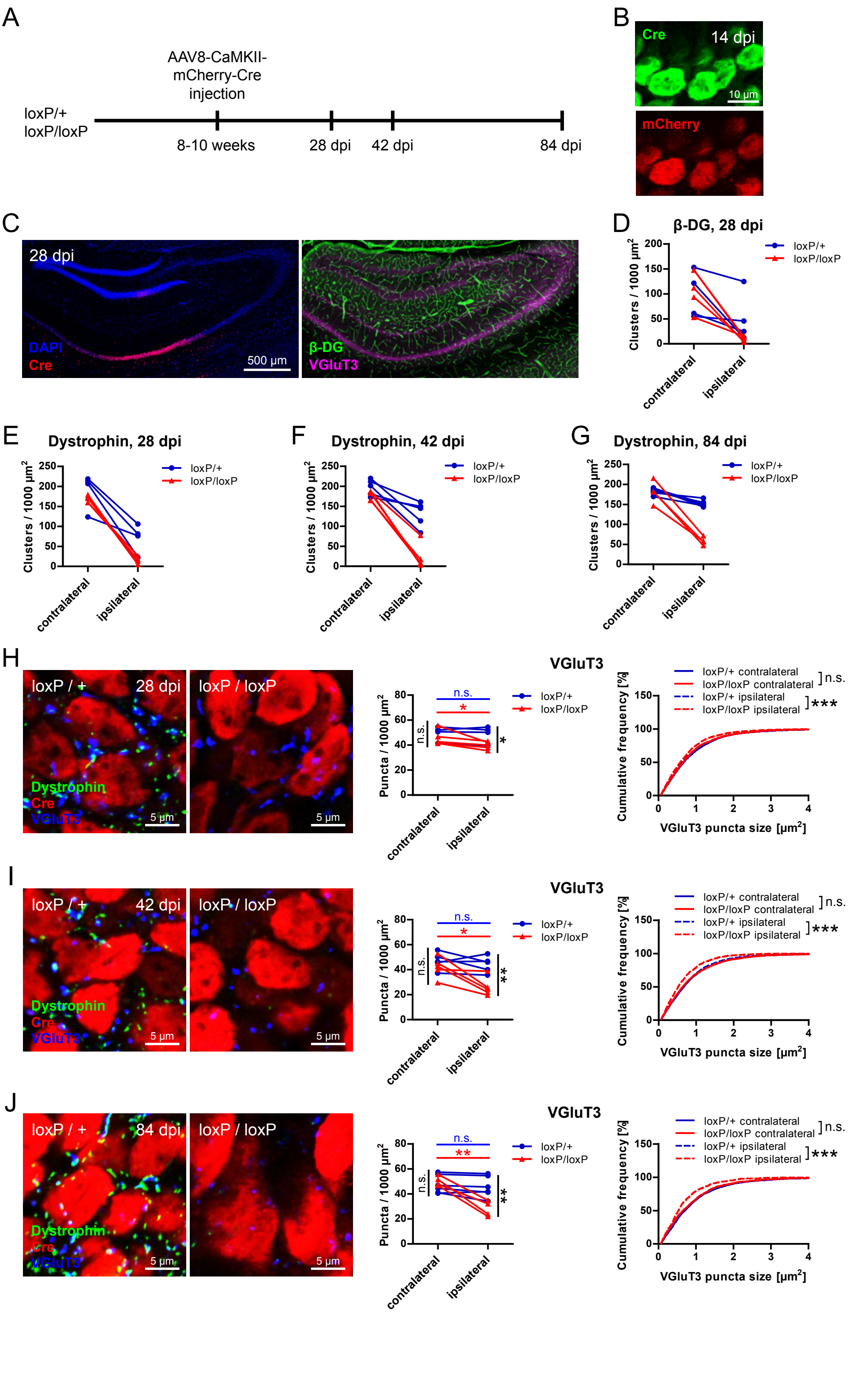
A
AAV8-CaMKII-
mCherry-Cre
injection
loxP/+
loxP/loxP
8-10 weeks
28 dpi
42 dpi
84 dpi
B
Cre
14 dpi
10 µm
mCherry
C
28 dpi
DAPI
Cre
500 µm
β-DG
VGluT3
D
β-DG, 28 dpi
Clusters / 1000 µm²
loxP/+
loxP/loxP
contralateral
ipsilateral
E
Dystrophin, 28 dpi
F
Dystrophin, 42 dpi
G
Dystrophin, 84 dpi
H
loxP / +
28 dpi
loxP / loxP
Dystrophin
Cre
VGluT3
5 µm
VGluT3
Puncta / 1000 µm²
n.s.
*
Cumulative frequency [%]
loxP/+ contralateral
loxP/loxP contralateral
loxP/+ ipsilateral
loxP/loxP ipsilateral
***
VGluT3 puncta size [µm²]
I
42 dpi
**
J
84 dpi
cre

Figure 9

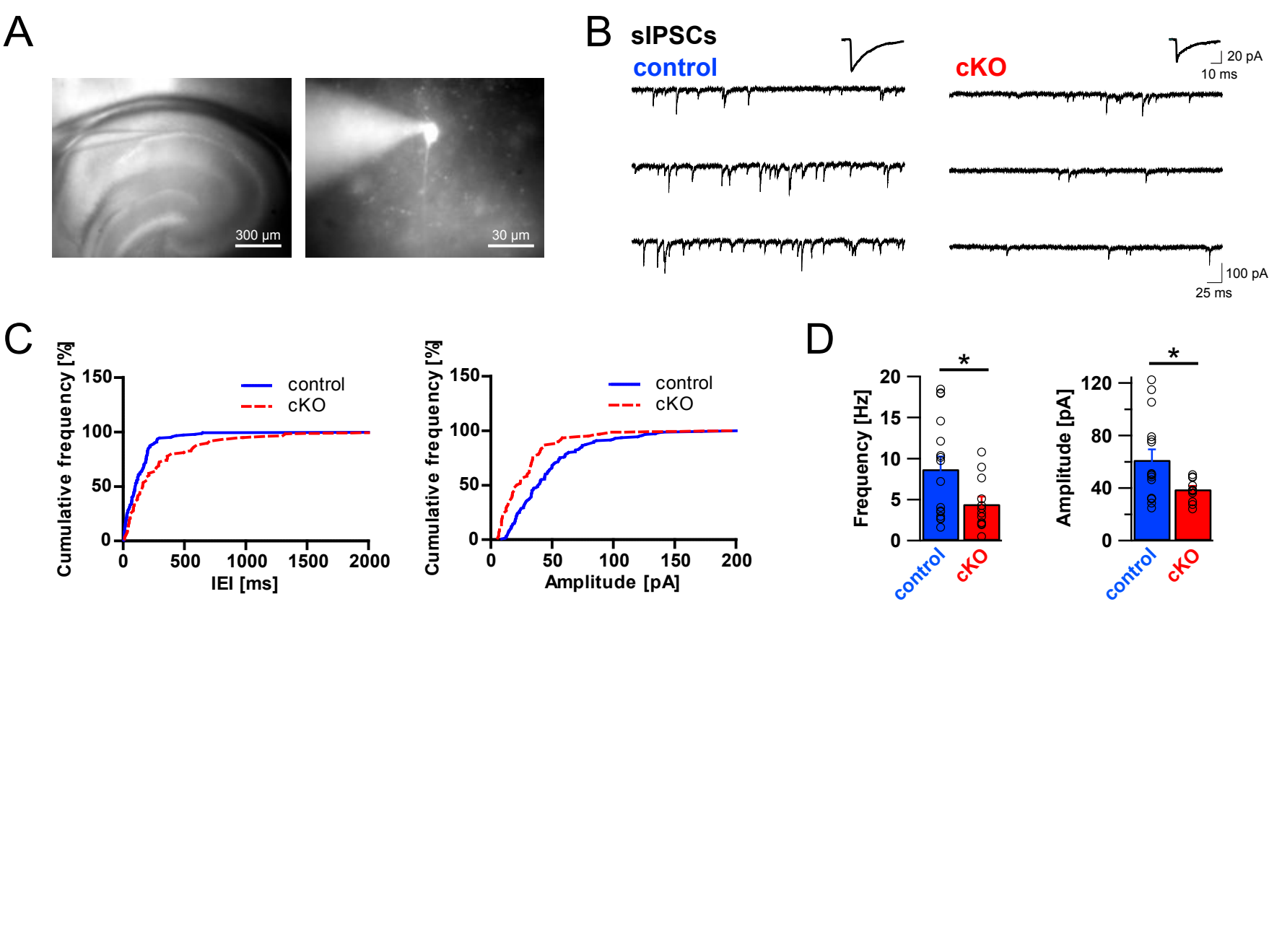
A
300 µm
30 µm
B
sIPSCs
control
cKO
20 pA
10 ms
100 pA
25 ms
C
Cumulative frequency [%]
150
100
50
0
0
500
1000
1500
2000
IEI [ms]
control
cKO
Cumulative frequency [%]
150
100
50
0
0
50
100
150
200
Amplitude [pA]
control
cKO
D
Frequency [Hz]
20
15
10
5
0
*
control
cKO
Amplitude [pA]
120
80
40
0
*
control
cKO

Figure 10

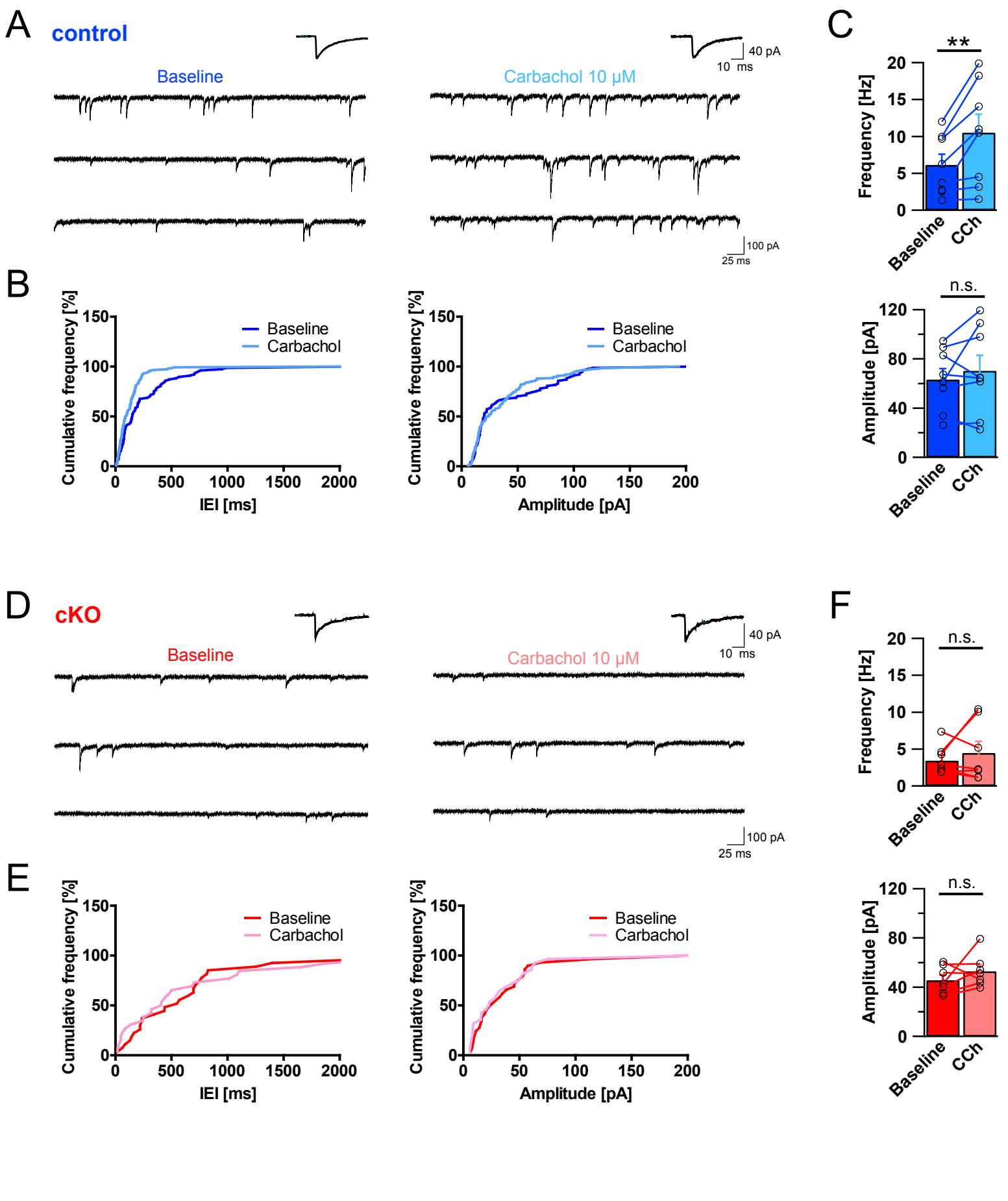
A
control
Baseline
Carbachol 10 µM
40 pA
10 ms
100 pA
25 ms
B
Cumulative frequency [%]
Baseline
Carbachol
IEI [ms]
Amplitude [pA]
C
Frequency [Hz]
**
Baseline
CCh
Amplitude [pA]
n.s.
D
cKO
E
F

Figure 11

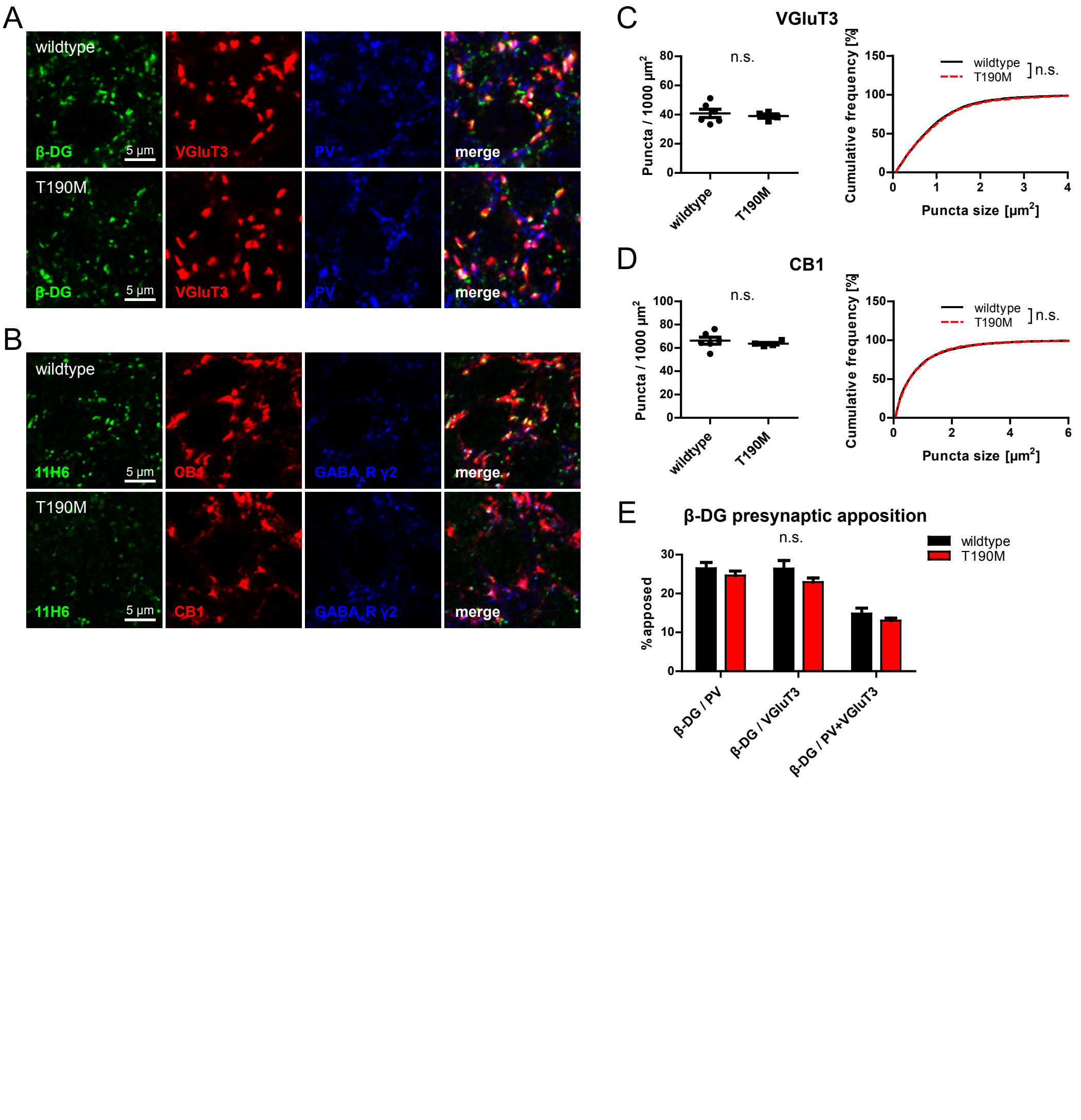
A
wildtype
β-DG
5 µm
VGluT3
PV
merge
T190M
β-DG
5 µm
VGluT3
PV
merge
B
wildtype
11H6
5 µm
CB1
GABA$_A$R γ2
merge
T190M
11H6
5 µm
CB1
GABA$_A$R γ2
merge
C
VGluT3
Puncta / 1000 µm^2
n.s.
wildtype
T190M
Cumulative frequency [%]
wildtype
T190M
n.s.
Puncta size [µm^2]
D
CB1
Puncta / 1000 µm^2
n.s.
wildtype
T190M
Cumulative frequency [%]
wildtype
T190M
n.s.
Puncta size [µm^2]
E
β-DG presynaptic apposition
n.s.
wildtype
T190M
% apposed
β-DG / PV
β-DG / VGluT3
β-DG / PV+VGluT3